Scientific report; WR-2002-06

NUSP-2
02-03

KNMI

ENVISAT Land Surface processes

Phase 2

Final report

B.J.J.M. van den Hurk, Z. Su, W. Verhoef, G. Roerink and L. Jia

Koninklijk Nederlands Meteorologisch Instituut

De Bilt, 2002

Scientific report = Wetenschappelijk Rapport; WR 2002-06

De Bilt, 2002

PO Box 201, 3730 AE De Bilt
The Netherlands
Wilhelminalaan 10
http://www.knmi.nl
Telephone +31 30 22 06 911
Telefax +31 30 22 10 407

Authors: B.J.J.M. van den Hurk, Z.Su, W. Verhoef, G. Roerink and L. Jia

This report describes a project carried out in the framework of the National User Support Programme 2001 - 2005 (NUSP-2) under responsibility of the Netherlands Agency for Aerospace Programmes (NIVR)

UDC: 551.507.362.2
528.8

ISSN: 0169-1651

ISBN: 90-369-2220-8

ENVISAT Land Surface processes Phase 2

Final report 4.2/AP-14

B.J.J.M. van den Hurk[1], Z. Su[2], W. Verhoef[3], G. Roerink[2] and L. Jia[2]

[1] KNMI, PO Box 201, 3730 AE De Bilt, The Netherlands
[2] Alterra, PO Box 125, 6700 AC Wageningen, The Netherlands
[3] National Aerospace Laboratory, Voorsterweg 31, 8316 PR Marknesse, The Netherlands

With further contributions from

M. Menenti[4], Z.-L. Li[4], Z. Wan[5] and A.F. Moene[6]

[4] GRTR/LSIIT, Université Louis Pasteur, Illkirch, France
[5] ICESS, University of California, Santa Barbara, USA
[6] Meteorology and Air Quality, Wageningen University, The Netherlands

NUSP-2 report 02-03
NUSP-2 project 4.2/AP-14

De Bilt/Wageningen, November 2002

This report describes a project carried out in the framework of the National User Support Programme 2001 – 2005 (NUSP-2) under responsibility of the Netherlands Agency for Aerospace Programmes (NIVR).

Contents

Acknowledgements

The work described in this report was supported by the Netherlands Remote Sensing Board (BCRS) under contract number 4.2/AP-14. For specific workpackages additional support was granted from the Netherlands Ministry of Agriculture, Nature Management and Fisheries (LNV), the Royal Netherlands Academy of Science (KNAW) and the NASA EOS Program contract NAS5-31370.

Abstract

Ths is a progress report of the 2nd phase of the project "ENVISAT- Land Surface Processes", which has a 3-year scope. In this project, preparative research is carried out aiming at the retrieval of land surface characteristics from the ENVISAT sensors MERIS and AATSR, for assimilation into a system for Numerical Weather Prediction (NWP). Where in the 1st phase a number of "first shot" experiments were carried out (aiming at gaining experience with the retrievals and data assimilation procedures), the current 2nd phase has put more emphasis on the assessment and improvement of the quality of the retrieved products. The forthcoming phase will be devoted mainly to the data assimilation experiments and the assessment of the added value of the future ENVISAT products for NWP forecast skill.

Referring to the retrieval of albedo, leaf area index and atmospheric corrections, preliminary radiative transfer calculations have been carried out that should enable the retrieval of these parameters once AATSR and MERIS data become available. However, much of this work is still to be carried out. An essential part of work in this area is the design and implementation of software that enables an efficient use of MODTRAN4 radiative transfer code, and during the current project phase familiarization with these new components has been achieved.

Significant progress has been made with the retrieval of component temperatures from directional ATSR-images, and the calculation of surface turbulent heat fluxes from these data. The impact of vegetation cover on the retrieved component temperatures appears manageable, and preliminary comparison of foliage temperature to air temperatures were encouranging. The calculation of surface fluxes using the SEBI concept,which includes a detailed model of the surface roughness ratio, appeared to give results that were in reasonable agreement with local measurements with scintillometer devices. The specification of the atmospheric boundary conditions appears a crucial component, and the use of first guess estimates from the RACMO models partially explains the succes.

Earlier data assimilation experiments with directional surface temperatures have been analysed a bit further and were also compared to results obtained from directly modeling the surface roughness ratio. Results between these calculations and the data assimilation results appeared well comparable, but a full test in which the surface roughness model is allowed to play a free role during the data assimilation process has yet to be carried out.

A considerable number of tasks that have yet to be carried out during Phase 3 has been formulated.

Introduction

The project "ENVISAT land surface processes" aims at the estimation of land surface properties that govern the turbulent exchange of energy and water vapour between the land surface and the atmosphere, anticipating on remote sensing observations that will become available after the launch of ENVISAT. The project is being carried out in the context of the User Support program of the Dutch Remote Sensing Committee (BCRS). It includes research aiming at defining optimal retrieval algorithms to derive characteristic land surface properties from remote sensing observations. In addition, assimilation of these observations in large scale atmospheric models is explored further.

The project is separated into three different consecutive phases. Phase 1 was finalised as described in the BCRS report USP-2 01/02 by Su and Jacobs (2001), covering activities carried out in 2000. Continuation of the project after the 1st phase was estimated to last an additional 2 years, as proposed in the proposal "ENVISAT Land Surface Processes Phase 2 & 3". Owing to the reorganisation of BCRS, only a limited portion of this 2-year continuation proposal was granted. The current document reports on this limited portion, labelled as Phase 2. This implies that a significant part of the work proposed in the continuation proposal is yet to be carried out, and we anticipate that this additional work will commence in a later stage during 2002.

A total of 9 workpackages were formulated in the continuation proposal:

0: Management and organisation
1: Surface albedo
2: Leaf area index
3: Retrieval of atmospheric parameters
4: Thermal emissivity
5: Directional surface temperatures
6: Sensible and latent heat fluxes
7: Assimilation of surface fluxes and moisture indicators in NWP
8: Validation of the improvements in the NWP predictions

In the next section progress in each of these workpackages is reported. No progress was made in workpackage 4 (thermal emissivity). In the next phase of the project, this workpackage will possibly be removed from the proposal. In Workpackage 5 contributions to a field experiment in China were included, and this is addressed in a separate section.

In the Executive Summary following the progress per workpackage, a brief summary of results (including a list of publications) is given, together with an outlook of work yet to be carried out.

Progress per Workpackage

WP 0: Project Management

B. van den Hurk

The work in the project was carried out at three different institutes: KNMI, Alterra and NLR. KNMI coordinated the project, which started at 1 April 2001. At the kick-off meeting, taking place at 19 April 2001, a detailed list of planned activities was established. At a progress meeting, taking place at NLR at 24 September 2000, progress per workpackage was reported by a number of scientific presentations, followed by discussions. Additional plans for the rest of the project period were established. Minutes of these meetings are included in the annexes.

Apart from these two meetings, work visits between KNMI and Alterra took place occasionally. These meetings focussed at the integration of the work in Workpackages 5 to 8, dealing with directional surface temperature retrieval, flux estimation and assimilation of these products into the KNMI atmospheric model.

The project management further consisted of preparation of financial and scientific reports submitted to BCRS.

Contribution to WP 1, 2 and 3: MODTRAN4 familiarisation

W. Verhoef

User interface

Because of the extensive spectral databases of solar irradiance and spectral absorption by atmospheric gases available in MODTRAN4 and the recently adopted DISORT method to calculate multiple scattering, this model has been selected as the software tool to compute the radiation interactions between the atmosphere and the earth's surface at hyperspectral resolution over the solar reflective spectral range. As the program MODTRAN4 has to be operated by specifying a complicated and precisely formatted ASCII control file, and a 97 page manual has to be studied before one might be able to produce such a control file successfully, it was decided to develop an easy-to-use graphical interface in Visual Basic on a PC. This interface is called Mod4U and is free downloadable from the site http://remotesensing.nlr.nl. Figure 0.1 below shows the "Card 5" tab form, in which the text window shows the currently specified coded inputs to MODTRAN4 as an ASCII file.

MODTRAN4 interrogation technique

By atmospheric scientists MODTRAN4 is considered to be a moderate spectral resolution model of radiative transfer in the atmosphere. However, for earth observation purposes this model represents nothing less than the state of the art, and the recent incorporation of the DISORT algorithm for accurate computations of atmospheric multiple scattering makes it a very suitable tool for realistic simulation and analysis of remote sensing problems in the optical and thermal spectral regions.

A problem with a model of this complexity is that its execution time is considerable, certainly if the DISORT option is selected. An alternative is using the much faster two-stream approximation of Isaacs *et al.* (1987), which is still available as an option and which was already applied in MODTRAN's predecessor LOWTRAN as well, but experience has shown that this method grossly underestimates the spherical albedo, especially at visible wavelengths. Although MODTRAN4 has new options (compared to previous versions) of including non-Lambertian targets (even various parametric BRDF models can be chosen) and targets differing from their surroundings, running this model pixel by pixel would still lead to prohibitive execution times. Therefore, it was decided to use an alternative approach, called "interrogation". This comes down to making a few runs with MODTRAN4 and then extracting spectra of six effective atmospheric parameters from the various output radiance results produced by the model. These six effective parameters are

ρ_{so}	=	TOA atmospheric bidirectional reflectance
ρ_{dd}	=	BOA spherical albedo of the atmosphere
τ_{ss}	=	direct atmospheric transmittance in the direction of the sun
τ_{oo}	=	direct atmospheric transmittance in the direction of viewing
τ_{sd}	=	diffuse atmospheric transmittance for solar incidence
τ_{do}	=	directional atmospheric transmittance for diffuse incidence

In order to be able to determine all six effective parameters it turns out to be sufficient to carry out only three MODTRAN4 runs, all for a uniform Lambertian surface reflectance, with spectrally flat surface albedos of 0%, 50% and 100% respectively. The MODTRAN outputs needed at each wavelength are PATH (total path radiance), GSUN (radiance contribution due to ground-reflected sunlight) and GTOT (total ground-reflected radiance contribution), as well as the extraterrestrial spectral solar irradiance. For PATH, the results obtained for 0% and 100% albedo are used, which are called $PATH_0$ and $PATH_{100}$, respectively. For GSUN only the output for 100% albedo is required ($GSUN_{100}$) and for GTOT one needs the outputs for 50% and 100%, called $GTOT_{50}$ and $GTOT_{100}$.

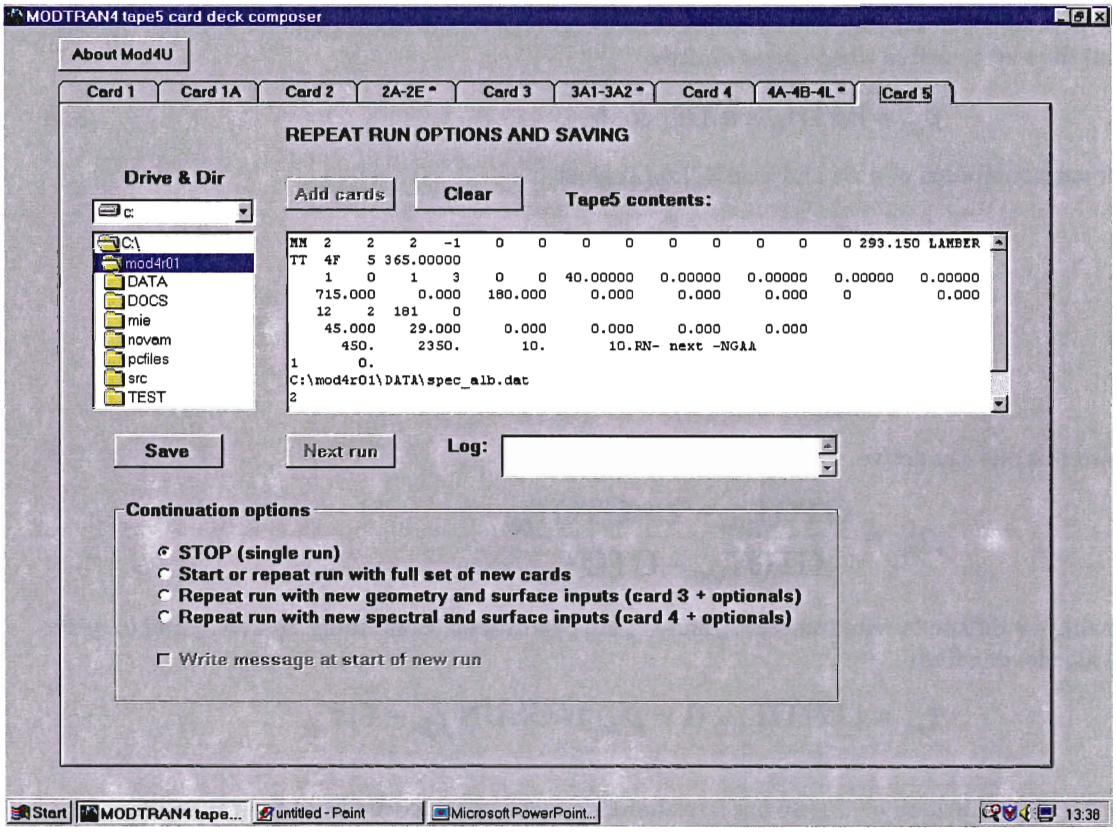

Fig. 0.1 Mod4U graphical user interface for preparing MODTRAN4 input control files

For the case of a uniform Lambertian surface with albedo a the planetary reflectance can be written as

$$r_p = \rho_{so} + \frac{(\tau_{ss}+\tau_{sd})\,a}{1-a\rho_{dd}}\tau_{do} + \frac{(\tau_{sd}+\tau_{ss}a\rho_{dd})}{1-a\rho_{dd}}a\tau_{oo} + \tau_{ss}a\tau_{oo} \quad , \qquad (0.1)$$

and the corresponding radiance contributions are given by

$$L_{PATH} = \left[\rho_{so} + \frac{(\tau_{ss}+\tau_{sd})\,a}{1-a\rho_{dd}}\tau_{do}\right]\frac{E_s^o}{}\cos\theta_s \quad ,$$

$$L_{GSUN} = \tau_{ss}a\tau_{oo}\frac{E_s^o}{}\cos\theta_s \quad , \text{ and} \qquad (0.2)$$

$$L_{GTOT} = \left[\frac{(\tau_{ss}+\tau_{sd})}{1-a\rho_{dd}}a\tau_{oo}\right]\frac{E_s^o}{}\cos\theta_s \quad .$$

The determination of the six atmospheric parameters from MODTRAN4 outputs now proceeds as follows. First, it is assumed that the direct transmittances obey Beer's law, so that one can write

$$\tau_{ss} = \exp(-b/\cos\theta_s) \quad \text{and} \quad \tau_{oo} = \exp(-b/\cos\theta_o) \quad , \qquad (0.3)$$

where b is the total optical thickness of the atmospheric layer, and θ_o is the zenith angle of observation. Deviations from Beer's law occur in strong water vapour absorption bands, but nevertheless one can still assume that in all spectral regions an effective optical thickness b can be determined by combining Eqs.(0.2) and (0.3) as

$$\tau_{ss}\tau_{oo} = \exp[-b(1/\cos\ _s + 1/\cos\theta_o)] = \mathrm{GSUN}_{100}\times\ /(E_s^o\cos\ _s) \quad .$$

Once b has been derived, Eqs.(0.2) can be applied to determine both direct transmittances separately.

The next step is to estimate the atmospheric bidirectional reflectance ρ_{so} and the spherical albedo ρ_{dd}. Eq.(0.2) for a zero surface albedo gives directly

$$\rho_{so} = \mathrm{PATH}_0 \times \pi / (E_s^o \cos\theta_s) \quad . \tag{0.4}$$

For surface albedos of 50% and 100%, Eq.(4) gives

$$\frac{(\ _{ss} + \tau_{sd})}{1 - 0.5\rho_{dd}} 0.5\tau_{oo} = \mathrm{GTOT}_{50} \times \ /(E_s^o \cos\ _s) \quad , \text{and}$$

$$\frac{(\ _{ss} + \tau_{sd})}{1 - \rho_{dd}} \tau_{oo} = \mathrm{GTOT}_{100} \times \ /(E_s^o \cos\ _s) \quad .$$

From this one can derive

$$\rho_{dd} = \frac{\mathrm{GTOT}_{100} - 2 \times \mathrm{GTOT}_{50}}{\mathrm{GTOT}_{100} - \mathrm{GTOT}_{50}} \quad .$$

Finally, the diffuse transmittances τ_{sd} and τ_{do} are determined. Combining Eqs. (0.2) and (0.3) for 100% albedo, one finds

$$\tau_{sd} = [\mathrm{GTOT}_{100}(1 - \rho_{dd}) / \mathrm{GSUN}_{100} - 1]\tau_{ss} \quad .$$

For the determination of τ_{do} we use a relationship that can be derived from Eqs.(2) and (4):

$$\frac{\mathrm{PATH}_{100} - \mathrm{PATH}_0}{\mathrm{GTOT}_{100}} = \frac{\tau_{do}}{\tau_{oo}} \quad , \text{ giving } \tau_{do} = \frac{\mathrm{PATH}_{100} - \mathrm{PATH}_0}{\mathrm{GTOT}_{100}} \tau_{oo} \quad .$$

Now all six effective atmospheric parameters have been determined. These are constant for each combination of geometric configuration and atmospheric state, but they have to be determined at each wavelength, so for a particular case one has to extract six spectra of the effective atmospheric parameters. By means of these "system" parameters one is able to model the effects of landscape heterogeneity and non-Lambertian surface reflection, although they were derived from the outputs of MODTRAN4 runs based on the assumption of a uniform Lambertian earth's surface. Figure 0.2 shows an example of spectra of the six effective atmosphere parameters from three MODTRAN4 runs.

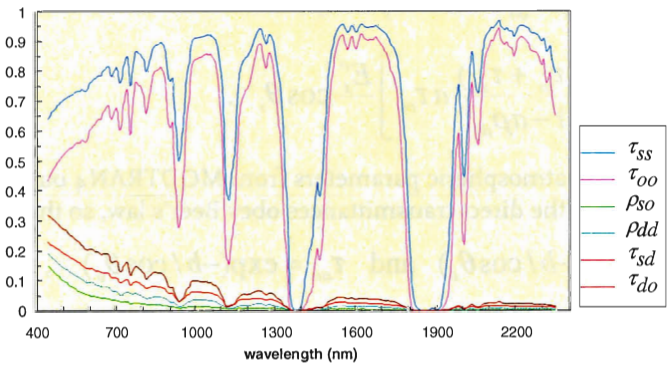

Fig. 0.2 Spectra of six effective parameters derived from MODTRAN4 outputs using interrogation technique

WP 1: Surface albedo (planned actions)

W. Verhoef

In the ESA project SASSSIS (Verhoef & Menenti, 1998) already a study on albedo estimation from multidirectional multispectral earth observations from space has been executed by means of the OSCAR (Optical Soil-Canopy-Atmosphere Radiance) model (Verhoef, 1998). In the LSPIM project this study was repeated for dual-look observations with the AATSR sensor. The results of both exercises indicated that albedo would be relatively easy to estimate with high accuracy by means of multiple linear regression equations when applied for each separate case given by the local solar zenith angle. However, when applied to actual AATSR observations of the Colmar site, the regression equations systematically overestimated the albedo values that were measured in the field. This might partly be caused by the large ground resolution cell size of the AATSR instrument, but another possible cause is the coarse spectral sampling of the SASSSIS simulation results. Only 7 spectral bands were simulated and the albedo was estimated by applying spectral weight factors to these bands in order to cover the response over the entire solar-reflective spectrum (400 – 2500 nm). The directional sampling was given by 28 directions spread over the hemisphere, and this should be considered amply sufficient to approximate the angular integral.

Recent activities performed in the framework of the DAASCEES project have learned that it is practically feasible to drastically improve the spectral sampling in model simulations by employing the models PROSPECT for the optical properties of single leaves and MODTRAN4 for realistic atmospheric radiative transfer calculations, both at hyperspectral resolution. Therefore, this combination of models offers greater potential for accurate albedo estimations, as the spectral integration can be significantly improved in this way. In the DAASCEES study the model GeoSAIL (Bach *et al.*, 2000) was used to simulate the surface BRDF and TOA radiances of vegetation pixels under various viewing directions. At each wavelength, six optical parameters derived from MODTRAN4 runs were used to model the interaction of the heterogeneous land surface with the atmosphere, including the so-called adjacency effect.

In order to perform realistic simulations for the sensors MERIS and AATSR on board of ENVISAT, a similar approach might be followed. However, in this case the ground resolution cell size is that large (300 m. or more), that the adjacency effect plays hardly a role, so the interaction with neighbouring resolution cells can be neglected, although the effects of intra-pixel heterogeneity should still not be overlooked of course. So the simulations can be limited to considering a series of (pure or mixed) ground objects, without having to take account of pixel-to-pixel heterogeneity.

In order to study the performance of surface albedo estimation by means of multiple linear regression it is proposed to simulate complete spectra of the directional reflectance on the ground for a number of representative objects and observational circumstances. These reflectance spectra are computed under the same 28 viewing directions as defined in the SASSSIS study, which will make it possible to obtain good estimates of the surface albedo.

For the same series of objects and observational circumstances, the TOA radiances as observed by MERIS and AATSR will be computed. These simulated observations are limited to the spectral bands of these sensors and constrained within orbital and instrumental (e.g. pointing range) boundary conditions. Next, by multiple linear regression analysis it can be investigated with which linear combinations of channels from MERIS and AATSR, and at which accuracy, it is possible to estimate the surface albedo.

Neither of these tasks has been completed in the current phase of the project. They will be included in the proposed continuation in Phase 3.

WP 2: Leaf area index

W. Verhoef

Principle and planned action

The leaf area index (LAI) of vegetated objects is a crucial parameter in the description of land surface processes. However, certainly for moderate spatial resolution sensors like MERIS and AATSR, the estimation of LAI is a problem because of the non-linear relation between LAI and surface reflectance. Especially in regions of moderate or strong absorption by vegetation (visible and mid-infrared parts of the spectrum) the canopy reflectance saturates above an LAI of about 2, and this causes a strong underestimation of LAI if the pixel is heterogeneous, which is almost exclusively the case at this spatial resolution. In the near infrared the absorption of radiation by leaves is much weaker, and in this spectral region the relation between LAI and canopy reflectance is closer to being linear, which means that also the estimation of LAI for mixed objects becomes less inaccurate. MERIS has several bands in the near infrared

and AATSR has one that can be employed in dual-look mode, so both instruments provide potentially new opportunities for more accurate LAI retrieval.

In the framework of the present project it is proposed to investigate the possibilities for LAI retrieval by means of multiple linear regression analysis. Because there is still some non-linearity in the relation between LAI and canopy reflectance, an attempt will be made to estimate exponentially transformed LAI-values of the form $\exp(-k\ LAI)$, where k is a coefficient that produces most closely a linear relation of transformed LAI with canopy reflectance in the near infrared. For a wavelength at 850 nm, with a minimum leaf absorption of about 0.04, this coefficient equals approximately 0.2.

It is proposed to combine the numerical experiment on LAI estimation with the one on surface albedo described above, so that both work packages can benefit from the same data base. The numerical experiment to be executed in order to create the required data base for the study of retrieval of both surface albedo and LAI is described in the next section.

Table 2.1 Number of values for each input parameter

Parameter	*Values*
Soil type	3
Soil moisture	2
Leaf C_{ab}	3
Leaf C_w	2
Leaf N	2
Canopy LIDF	3
Canopy LAI	10
Canopy hot spot par.	4
Atmospheric visibility	3
Water vapour	2
Solar zenith	3
View zenith	4
View azimuth	7

Numerical experiment

In the SASSSIS study all simulated observations, comprising 28 viewing directions in 7 spectral bands, were stored in a data base, which was used as a starting point for multiple linear regression statistical analysis. Surface reflectance factors as well as planetary (top-of-atmosphere) reflectances were computed by means of the OSCAR model, and the whole data base was searched in order to find the best combinations of spectral bands and viewing directions for the retrieval of surface albedo and LAI. By the combination of the models PROSPECT, SAILH and MODTRAN4 it is now possible to drastically increase the spectral sampling of canopy and soil reflectances, as well as of atmospheric transmission. In principle this allows a much more accurate estimation of surface albedo and calculation of in-band observed radiances for virtually any optical instrument for which the spectral bands are known. However, at 10 nm spectral resolution each spectrum contains more than 200 values, so storage requirements would be considerable if for all possible combinations of object and atmosphere the radiance spectra were to be stored in a data base. For example, in the case of, say, 9000 different ground objects (combinations of soil, leaf type and canopy architecture) and 6 atmospheric states more than 600 Mbytes of information would have to be stored for each solar zenith angle. Therefore, an alternative is proposed. In this solution 334 Mbytes of information on hyperspectral surface reflectance of 8640 ground objects is stored in a database, besides 2.5 Mbytes of hyperspectral information on the six parameters describing the effective optical behaviour of the atmosphere. So ground surface and atmosphere are decoupled, and by this intervention the large number of possible combinations of ground object and atmospheric state does no longer require the equivalent amount of storage space.

Now, for the same series of objects and atmospheric states (including solar zenith angle) radiance observations for the specific MERIS and AATSR sensors can be simulated, while the data base is used to compute the corresponding surface albedos. Table 2.1 summarises for each parameter the number of cases that are proposed to be simulated for the modelling of surface albedo. In total, this comprises 6 soils, 12 leaves and 120 canopy architectures (8640 objects), 6 atmospheric states, 3 solar zenith angles and 28 directions of view.

WP 3: Retrieval of atmospheric parameters

W. Verhoef

The MERIS instrument offers several possibilities for applying differential absorption techniques to estimate local atmospheric parameters such as total water vapour column and aerosol optical thickness, also over land. For MERIS seven spectral bands (9 to 15) have been defined in the near infrared region. Band 9 and bands 12 to 15 are to various degrees influenced by water vapour absorption, band 11 by oxygen absorption and band 10 by no absorption at all. Bands 10 and 11 are intended to be used in combination in order to provide estimates of surface pressure (or terrain height), as the oxygen absorption in band 11 varies with surface pressure. Here band 10 is used as a reference. For flat terrain or known surface height these bands might be used to estimate local aerosol optical thickness, as in a clear atmosphere the relative effect of oxygen absorption in band 11 compared to band 10 is different from the effect in a hazy atmosphere. This is illustrated in Fig. 3.1 for visibilities of 40 km (clear) and 10 km (hazy). For both situations the planetary reflectances in both bands are shown for the series of surface albedo values of 0, 0.1,..., 1.0. The planetary reflectances in the oxygen absorption band (761 nm) have been multiplied by 16 in order to obtain comparable signals. The difference in wavelength is so small that one can safely assume that the surface reflectances in both bands are equal, and a scatterplot becomes a narrow line if visibility is constant. Yet the slope of this line changes under influence of aerosol optical thickness, which is caused by the different vertical density profiles of air (oxygen) and aerosols, as the latter are more concentrated in the lower layers. Contrary to other methods, that work better for dark backgrounds (e.g. dark dense vegetation in the visible, clear water bodies in the near infrared), this method works best for relatively bright backgrounds, as otherwise the difference in vertical profiles between a clear and a hazy atmosphere remains largely unnoticeable. This means that for vegetated land surfaces the method might work reasonably well, contrary to other methods that work only over dark surfaces.

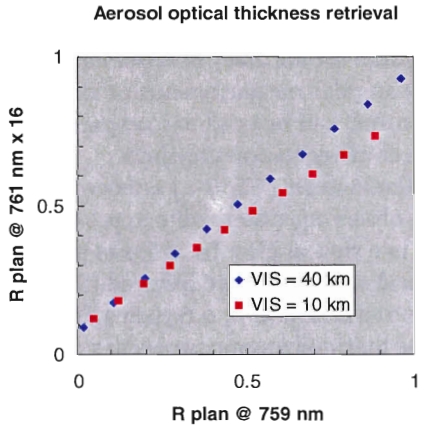

Fig. 3.1. Scatterplot of representative planetary reflectances outside and inside the oxygen absorption band (MERIS bands 10 and 11) for two visibilities, computed by MODTRAN4.

WP 4: Thermal emissivity

No progress was made in this workpackage. It is anticipated that this workpackage will be eliminated from the next phase of the project, since substantial progress in this area is not expected to result from the limited resources devoted to this work.

WP 5: Directional radiometric surface temperatures

Since the resistance to heat transfer between land surface and atmosphere can be shown to depend on the two vegetation and soil surface temperatures, determination of these temperatures becomes a major issue for land surface processes. The only way to retrieve these quantities from satellite data is through inverse modeling of directional TIR radiance. (A)ATSR offers the possibility to invert the two nadir and forward measurements and get T_{soil} and T_{veg}, provided ancillary information is available to describe the complex target. Since inverse modeling must be applied quantities at the bottom of the atmosphere, atmospheric corrections of TOA radiance must be performed first.

The output of the WP was anticipated as an algorithm to determine T_{soil} and T_{veg} with (A)ATSR data. The enclosed contribution by Jia et al., (2001) 'A practical algorithm to infer soil and foliage component temperatures from bi-angular ATSR-2 data' provides details of the work performed.

A dataset has been obtained from a field campaign in Shunyi near Beijing, China from March to April 2001. The purpose of the project team to participate in the campaign was to collect relevant data for the validation of the retrieval of component temperatures, emissivity and sensible and latent heat fluxes estimation using satellite data. Due to the huge amount of work involved in pre-processing of the data, especially the in-situ as well as air-borne radiometric data, the detailed analysis and reporting of the results will be the tasks of the Phase 3 of the project. A brief description of the observation instruments and some example data sets are given in the subsequent section.

A practical algorithm to infer soil and foliage component temperatures from bi-angular ATSR-2 data

Li Jia, Zhao-Liang Li, Massimo Menenti, Zhongbo Su, Wout Verhoefand Zhengming Wan
(Submitted to *International Journal of Remote Sensing*)

Introduction

A mixture of soil and vegetation is an important category of land surfaces over which significant angular variations in thermal infrared radiance (TIR) are observed (Kimes 1980, Nielsen et al. 1984, Lagouarde et al. 1995). The architecture of vegetation canopies leads to significant variability of radiative and convective energy fluxes in the canopy space. The latter implies significant thermal heterogeneity and, with that, changes of the observed surface temperature with view angle. Studies based on model simulations and field measurements show large angular variations of the brightness surface temperatures (Kimes 1983, Sobrino and Caselles 1990, Prévot et al. 1993, Smith et al. 1996), which may be usable to infer vegetation and soil temperatures (Kimes and Kirchner 1983).

However, angular changes in exitance may be relatively small, so only observations at very different angles give a signal significantly larger than the accuracy of observations. This limits to very few the number of significant and independent angular measurements of exitance, which implies that only very simple models (i.e. with very few unknowns) can be used to interpret the observations and to obtain estimates of the component temperatures of vegetation canopies.

The second Along-Track Scanning Radiometer (ATSR-2) onboard the European Remote Sensing satellite (ERS) is currently the only one observing system able to provide quasi-simultaneous multispectral (from visible to TIR) measurements at two view angles. In addition to three thermal infrared channels centered at 3.7μm, 11μm and 12μm and one short wave infrared (SWIR) channel at 1.6μm, ATSR-2 has three visible-near infrared channels centred at 0.56μm, 0.67μm and 0.87μm intended for vegetation analysis. Such data provide access to the thermodynamic properties of soil – foliage mixtures over larger area of land surface. Improvement of land surface process models is feasible through the use of the improved visible and near infrared atmospheric corrections and the separate retrievals of different component (soil and foliage) temperatures in a pixel (Jia et al. 2001, van den Hurk et al. 2001).

In this study, an operational algorithm is developed to retrieve soil and foliage temperature over heterogeneous land surface based on the analysis of bi-angular and multi-channels observations made by ATSR-2. Limitations and uncertainties in retrieving component temperatures using the present algorithm are discussed through several case studies.

Methodology

Inversion of a simple linear model of thermal infrared radiation of foliage-soil mixture

A soil-vegetation system composed of foliage and soil is characterized by large temperature differences within the canopy space. Besides the 'angular emissivity' effects for such system, directionality of TIR radiance will appear because of the thermal heterogeneity and the three-dimensional (3-D) structure of the system. The surface radiometric temperature measured by a radiometer varies with the zenith view angle of the radiometer since different proportions of elements fill in the instantaneous field of view (IFOV) of the sensor at different zenith view angles.

This anisotropy of exitance, on one hand, brings a difficulty in obtaining a reliable surface temperature measurement, on the other hand, provides an opportunity to extract component temperatures of the surface elements. The radiance measured by a radiometer is contributed by the emittances of the targets viewed in the IFOV of the radiometer (and by the emittance from the surrounding). Therefore, the radiance measured by a radiometer can be related to the radiances from each element by weighing their emittance with the

fraction of IFOV. Considering a canopy system with soil and foliage components, such relationship can be expressed by a simple linear radiation transfer model (Li et al. 2001a, Menenti et al. 2001),

$$B(T_{rad}(\theta)) = F(\theta)\varepsilon_f(\theta)B(T_f) + (1-F(\theta))\varepsilon_s(\theta)B(T_s) \qquad (5.1)$$

where B is Planck function; T_{rad} is the radiometric surface temperature at ground level; θ is the view angle of the radiometer; $F(\theta)$ is the fractional cover of foliage; $\varepsilon_f(\theta)$ is the effective emissivity of foliage; T_f is foliage temperature; $(1-F(\theta))$ is the fractional cover of soil; $\varepsilon_s(\theta)$ is the effective soil emissivity; T_s is soil temperature. In this inversion model (equation 5.1), we have assumed that: 1) foliage has a constant temperature T_f ; 2) both the soil and the foliage surfaces are Lambertian; 3) the effective emissivity of soil and foliage are used due to the consideration of the interaction between vegetation-soil and vegetation-vegetation (see Li et al. 2001a).

With radiance measurements at two view angles (i.e.. obtained by ATSR-2 at nadir and forward view angles), equation 5.1 can be rewritten (for a given spectral range) as two equations for each pixel, making it possible to derive two component temperatures T_s and T_f. In a previous study (Menenti et al, 2001), we used a different approach. We wrote equation 5.1 for two zenith view angles and two wavelengths to retrieve T_s, T_f and LAI. This former approach required:

- to perform atmospheric correction for each TIR channel and view angle using the MODTRAN4 code and rediosoings;
- to assume the values of soil and foliage spectral emissivities at both wavelength.

These assumptions made the approach less robust and led us to the idea of developing the algorithm described in this paper.

One should note that in principle there are at least four component temperatures in the IFOV: 1) sunlit foliage, 2) shaded foliage, 3) sunlit soil, 4) shaded soil. However, it is impossible to get these four component temperatures simultaneously from only bi-angular measurements and multi-angular observations would be necessary for this purpose. Therefore, the soil and foliage temperatures obtained using equation 5.1 should be considered as the effective soil (the mixture of sunlit and shadowed soil) and effective foliage (the mixture of sunlit and shadowed foliage) temperatures. Moreover, to reduce the unknowns in equation 5.1, the emissivity angular effect has been neglected due to the cavity effects (Li et al., 2001a) so that

$$\varepsilon_s(\theta_1) = \varepsilon_s(\theta_2) = \varepsilon_s \text{ and } \varepsilon_f(\theta_1) = \varepsilon_f(\theta_2) = \varepsilon_f$$

With these assumptions, the directional radiance measured at ground level comes only from the emitance of soil and foliage existing in the IFOV in the direction θ

$$B(T_{rad}(\theta)) = F(\theta)\varepsilon_f B(T_f) + (1-F(\theta))\varepsilon_s B(T_s) \qquad (5.2)$$

Equation 5.2 is used to infer soil and foliage component temperatures T_s and T_f provided that the vegetation fractional cover can be estimated from visible and near infrared reflectances and ε_f and ε_s are known.

Determination of vegetation fraction cover F(θ)

To retrieve soil and foliage temperatures from equation 5.2, the viewing angle-dependent vegetation fraction needs to be determined independently from additional observation. Two different approaches were applied in this study to estimate the fractional vegetation cover using visible and near infrared data. Both have drawbacks and are based on a set of assumptions, which require evaluation.

Baret et al. (1995) have established a semi-empirical relationship between vegetation fraction and spectral vegetation indices such as $NDVI$, i.e.

$$F(\theta) = 1 - \left(\frac{NDVI(\theta) - NDVI(\theta)_{\max}}{NDVI(\theta)_{\min} - NDVI(\theta)_{\max}} \right)^K \qquad (5.3)$$

where $NDVI(\theta)_{\max}$ and $NDVI(\theta)_{\min}$ are the vegetation index after atmospheric corrections for infinite leaf area index (LAI) and for the bare soil ($LAI = 0$), respectively. Using a radiative transfer model , these authors found $NDVI_{\min} = 0.0151$, $NDVI_{\max} = 0.8858$ and $K = 0.4631$.

Another approach to estimate $F(\theta)$ from surface reflectances $\rho_i(\theta_s, \theta, \Delta\phi)$) is to use the stepwise multiple linear regression

$$F(\theta) = a_0(\theta_s, \theta) + \sum_{i=1}^{n} a_i(\theta_s, \theta)\rho_i(\theta_s, \theta, \Delta\phi) \quad (5.4)$$

where n is the number of channels used in the range of visible to SWIR channels, θ_s is solar zenith angle, $\Delta\phi$ is the relative azimuth angle between sun and satellite direction. The model OSCAR (Verhoef 1998) has been applied to generate surface reflectances for the viewing and illumination conditions applying to the ATSR-2 observations used in this study and to an ensemble of canopy and atmospheric conditions. Reflectances in the three optical bands (green, red and NIR) have been simulated for nadir view and a zenith view angle of 53 degrees. The relative azimuth angle was roughly estimated to be equal to 120 degrees.

It should be noted that the coefficients a_i in equation 5.4 apply to the ensemble of conditions simulated with OSCAR. These conditions comprise the variation over ten LAI values, three leaf inclination distribution function (LIDF), four hot spot parameters, four types of leaf, four types of soil, four surroundings which consist of a simple description of the terrain surrounding the target, three atmospheric visibilities and five solar zenith angles. The LAI values range from 0 to 6. The three LIDFs are representative for moderately planophile (most leaves having 25° inclination), plagiophile (most leaves having 45° inclination) and moderately erectophile (most leaves having 65° inclination) canopies, respectively. The hot spot size parameter q is the ratio of the horizontal correlation length of leaf projections and the height of the canopy layer. The series of q values are taken as 0.05, 0.10, 0.20 and 0.50. Spectrally different leaf types were taken from the literature (Gausman et al., 1978). Spectral reflectance data of four soil types were taken from atmospherically corrected Landsat Thematic Mapper images of the Netherlands (1986), supplemented with data for the spectral band at 1250 nm. The three atmospheric visibility conditions were taken as 5, 10, and 40 km (see Verhoef 1998, Verhoef and Menenti 1998, Verhoef 2001 for the details).

For all combinations of the above conditions (115 200 cases in total) the reflectance was computed in the three ATSR-2 bands in the two directions, at the surface level. Table 5.1 gives the values of regression coefficients in the different solar zenith angles (θ_s) and the correlation coefficients R^2 which is the measure of the quality of parameter retrieval. The coefficients in table 5.1 are then interpolated to each ATSR-2 pixel according to the solar zenith angle for each pixel.

Table 5.1: The regression coefficients in the stepwise multiple linear regression (equation (4)) generated by OSCAR model at different solar zenith angle (θ_s). R^2 is the square of correlation coefficients.

	θ_s (°)	a_0	a_1	a_2	a_3	R^2
F(nadir)	15	0.1684	0.94	-3.79	1.46	92.0
	30	0.1550	0.92	-3.84	1.51	92.3
	45	0.1239	0.90	-3.79	1.58	92.7
	60	0.0762	0.69	-3.53	1.67	93.0
	75	0.0388	0.19	-3.12	1.75	92.6
F(Forward)	15	0.2213	1.05	-4.26	1.50	90.3
	30	0.2045	1.02	-4.21	1.54	91.2
	45	0.1660	0.98	-4.05	1.59	92.6
	60	0.1066	0.80	-3.67	1.65	93.7
	75	0.0447	0.38	-3.14	1.71	93.9

Atmospheric corrections

Column water vapour determination

Column water vapor content in the atmosphere plays an important role in the atmospheric corrections in visible, near infrared and thermal infrared channels. Because water vapor varies rapidly in time and space, the radiosoundings made at one place and at one time are generally not representative for the whole

image. It is therefore desirable to retrieve water vapor content directly from satellite data. Several methods have been proposed and developed for different instruments (Klesspies and McMillin 1990, Sobrino et al. 1994). An operational algorithm of deriving water vapor content from two thermal channels of ATSR-2 has been developed by Li et al. (2001b) which is used in this study.

Atmospheric corrections in thermal infrared channels

To obtain the surface temperature at the bottom of atmosphere (BOA), atmospheric correction is needed for the correction of the atmospheric effects on the radiance measured at the top of atmosphere (TOA). Following the procedure developed by Becker and Li (1995), a general split-window (SW) algorithm depending explicitly on the total column water vapor content in the atmosphere (W) is derived for ATSR-2 nadir and forward views:

$$T_{rad}(\theta) = [a(\theta) + b(\theta)W] + [c(\theta) + d(\theta)W]T_{11}(\theta) + [e(\theta) + f(\theta)W][T_{11}(\theta) - T_{12}(\theta)] \quad (5.5)$$

where T_{rad} is the brightness surface temperatures at the ground level; θ is the view angle of ATSR-2; T_{11} and T_{12} are the brightness temperatures at TOA measured by ATSR-2 at 11μm and 12μm channels, respectively. For the large range of surface parameters and atmospheric conditions ($W \leq 4.5g/cm^2$, air temperature at surface T_a, $272\text{K} \leq T_a \leq 311\text{K}$ and $-5\text{ K} \leq T_{rad} - T_a \leq 15\text{K}$), the coefficients $a \sim f$ have been generated for ATSR-2 nadir and forward views (see table 5.2).

Atmospheric corrections in visible and near infrared channel

Atmospheric perturbations (mainly due to absorption and scattering processes) are responsible for substantial modifications of the surface spectral reflectance measured by satellite instruments. It is therefore necessary to correct for the atmospheric effects to retrieve the surface reflectance. Methods of atmospheric corrections are generally concerned with the estimation of the atmospheric effects associated with molecular absorption, molecular and aerosol scattering. Current methods for the estimation of the atmospheric effects employ a radiative transfer model (Vermote et al. 1997, Beck et al. 1999) whose inputs are generally the vertically integrated gaseous contents, aerosol optical properties and geometric conditions.

Table 5.2: The coefficients of Split-window method (equation 5.5) to invert surface temperature from ATSR-2 thermal infrared channels at nadir and forward view angles. σ is the root mean square (RMS) residual of surface temperature retrieval.

	a	b	c	d	e	f	σ (K)
Nadir	-4.89	3.74	1.0205	-0.0151	0.916	0.509	0.10
Forward	-14.41	8.51	1.0582	-0.0343	0.565	0.857	0.24

If ρ_i^* is the reflectance measured in channel i at the top of atmosphere (TOA), from radiative transfer theory, the surface reflectance in channel i, ρ_i, can be expressed as (Rahman and Dedieu 1994, Vermote et al. 1997)

$$\rho_i(\theta_s, \theta, \Delta\phi) = \frac{\rho_i^{ac}(\theta_s, \theta, \Delta\phi)}{1 + S_i \rho_i^{ac}(\theta_s, \theta, \Delta\phi)} \quad (5.6)$$

with

$$\rho_i^{ac} = \frac{\rho_i^*(\theta_s, \theta, \Delta\phi)/tg_i(\theta_s, \theta) - \rho_i^a(\theta_s, \theta, \Delta\phi)}{t_i(\theta_s)t_i(\theta)}$$

where S_i is the spherical albedo of atmosphere in channel i. tg_i is the total gaseous transmission in channel i associated with gaseous absorption along the sun-target-sensor atmospheric path. $\rho_i^a(\theta_s, \theta, \Delta\phi)$ is the atmospheric reflectance. $t_i(\theta_s)$ and $t_i(\theta)$ are the total atmospheric transmittance along the sun-target and target-sensor atmospheric paths, respectively.

In general, the independent measurements of atmospheric composition and aerosol optical properties are not available; it is therefore desirable to derive them directly from satellite data. The most important gases for atmospheric corrections in the visible and near infrared channels are water vapor and ozone.

Water vapor content in the atmosphere may be derived from the two split-window channel measurements as shown above, and ozone content is taken from climatological data. As for the determination of the aerosol optical properties, if the surface reflectance may be considered isotropic, then the difference in surface reflectance retrieved from multi-angle directions using equation 5.6 may be used to derive the atmospheric optical thickness if aerosol type is assumed. However, most land surfaces are far from Lambertian (Hapke, 1981). With multi-angle measurements, it is imperative to consider non-Lambertian reflectance. Several multi-look aerosol retrieval schemes for ATSR-2 have been proposed (Flowerdew and Haigh 1997, Mackay and Steven 1998, North et al. 1999). The simplest one relies on the assumption that the functional shape of the bidirectional effects is invariant with respect to the wavelength within the visible and near-infrared region (Flowerdew and Haigh 1997, Mackay and Steven 1998, North et al. 1999).

$$\frac{\rho_i(\theta_1)}{\rho_i(\theta_2)} = \frac{\rho_j(\theta_1)}{\rho_j(\theta_2)} \tag{5.7}$$

This relationship gives a constraint for atmospheric correction by forcing the retrieved at-surface bidirectional reflectances in channel i and j to have a consistent angular variation, even though the magnitude of the reflectance in two channels may be very different.

The aerosol optical thickness is therefore obtained through the minimization of the error matrix function

$$E = \sum_{i=1}^{4}\sum_{j>i}^{4}\left(\frac{\rho_i(\theta_1)}{\rho_i(\theta_2)} - \frac{\rho_j(\theta_1)}{\rho_j(\theta_2)}\right)^2 \tag{5.8}$$

where i and j are channel numbers and n is the total number of channel used ($n \leq 4$ for ATSR-2).

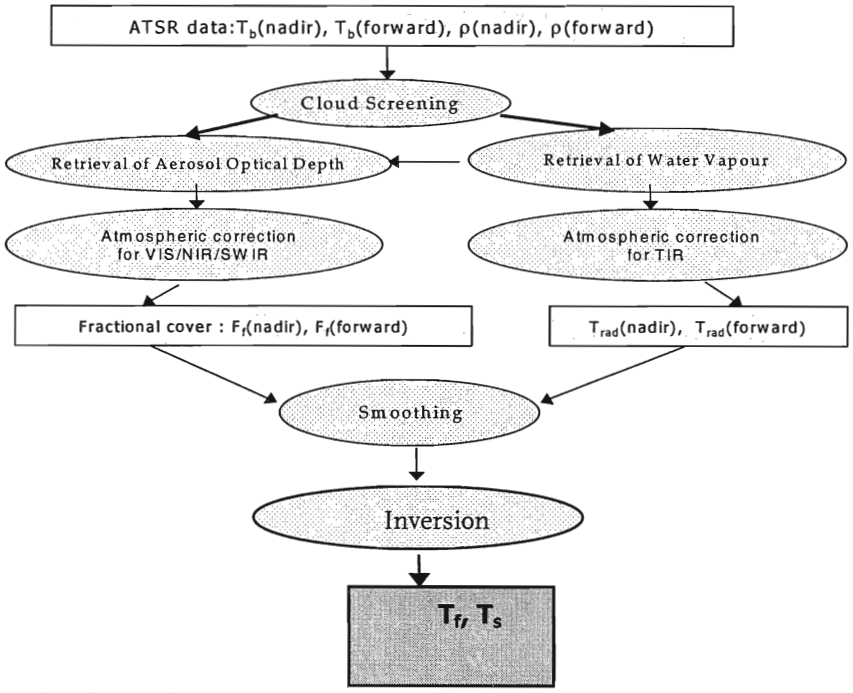

Fig. 5.1: The scheme of the operational algorithm for retrieval of T_f (foliage temperature) and T_s (soil temperature) from ATSR multi-spectral and dual-angular measurements. T_b: brightness surface temperature at TOA measured by TIR channels of ATSR-2; ρ: reflectance at TOA measured by VIS/NIR/SWIR channels of ATSR-2; T_{rad}: surface temperature at BOA.

Operational Implementation

To apply the inversion model described above to ATSR-2 multi-spectral and bi-angular measurements, several pre-processing steps are needed to obtain the input variables required in equation 5.2. For instance, the ATSR-2 measures radiance at TOA, which includes the atmospheric effects. Atmospheric corrections

are needed to obtain the BOA values for each channel measurement. A general scheme of the ATSR-2 data processing procedures is shown in figure 5.1, composed of 8 steps.

Cloud and water surface screening

The cloud screening algorithm is based on the threshold method proposed by Saunders and Kriebel (1988) and is adapted to ATSR-2. Threshold values are subjectively determined for each image based on ATSR-2 visible and infrared data. Moreover, pixels in which the TIR sensors are saturated (approximately > 319 K) are screened. Finally water pixels are screened out, since the separation of soil and foliage temperatures is not relevant in these cases.

Water Vapor Determination

After the cloud and water screening procedures, a box size of $m \times n$ ($N = m \times n$) has to be defined so that the algorithm developed by Li et al. (2001b) to retrieve water vapor content can be applied to each box area. The choice of the box size is somewhat arbitrary. In the current study, the size of the box was 10×10 ($N = 100$) pixels. Readers interested to the detailed procedures are referred to Li et al. (2001b).

Retrieval of aerosol optical depth

Retrieval of the aerosol optical depth is performed by aggregating the top of atmosphere data for a box of 10×10 pixels to minimize noise and the effect of misregistration between the two views and to reduce the computing time. Given an initial estimate of aerosol optical depth at 550nm, τ^a_{550}, the water vapor content W retrieved as described in section 4.2 and the climatological ozone content, initial estimates of land surface reflectances are obtained by inversion of atmospheric model 6S (Second Simulation of the Satellite Signal in the Solar Spectrum, Vermote et al. 1997) for each set of ATSR-2 observations. The degree of fit of this set of reflectances to the land surface bi-directional reflectance model (equation 5.7) gives an error matrix as shown in equation (5.8), which is minimized using the Levenberg-Marquardt algorithm (Press et al. 1989) with simple bounds on variables ($0.1 \leq \tau^a_{550} \leq 0.7$, $0 \leq \rho_i \leq 1.0$).

Atmospheric corrections in the visible and near infrared channels

Knowing the water vapor content (W) and aerosol loading (τ^a_{550}) in the atmosphere, the atmospheric correction is performed on a pixel by pixel basis to get the land surface reflectances at the BOA for all visible and near infrared channels and for all viewing angles. It should be noted that for clear pixels within the box in which water vapor and aerosol loading cannot be retrieved, atmospheric correction for these pixels is performed with the mean water vapor content and mean aerosol loading over the whole image.

Estimation of Fractional vegetation cover

Estimation of fractional vegetation cover is performed on a pixel-by-pixel basis using either equation 5.3 or equation 5.4. Equation 5.3 is calculated using $NDVI_{min}$ and $NDVI_{max}$ values determined for each image, i.e., as the minimum and maximum values of the atmospherically corrected NDVI image. We did not use the theoretical values given by Baret et al (1995) for two reasons:

1. The ATSR-2 spectral channels (see website at: `http://www.atsr.rl.ac.uk/documentation/docs/userguide/index.shtml`) differ in position and bandwith from the spectral channels chosen by Baret et al (1995); this difference has an impact on the $NDVI_{min}$ and $NDVI_{max}$ values;
2. The values given by Baret et al (1995) were obtained by model calculations on the basis of assumed spectral reflectances for green leaves and soil which may be different from those in the study areas. For the area with yellow and brown leaves, for instance, fractional vegetation cover maybe relatively high while the values of NDVI remain relatively smaller.

Atmospheric corrections in thermal infrared channels-split window method

Given the water vapor content in the atmosphere, surface brightness temperature T_{rad} is directly derived on a pixel-by-pixel basis with equation (5) for both nadir and forward views. As in step 4.4, for clear pixels within the box in which water vapor content is not available, the mean water vapor content in the whole image is used in equation 4.5.

4.7 Smoothing

The bi-angular ATSR-2 observations may be affected by co-registration errors and by the different footprint between nadir and forward views. To reduce the impact on the soil and foliage temperature separation, a local moving window filter of 5×5 pixels for the nadir image and of 3×3 pixels for the

forward view image were applied over the whole image. Window size was chosen taking into account the different spatial resolution of nadir and forward views ($1km \times 1km$ for nadir view, $1.5km \times 2km$ for forward view).

Separation of soil and foliage component temperatures

Soil and foliage component temperatures are derived from two surface brightness temperatures T_{rad}, equation 5.2, using the Levenberg-Marquardt algorithm (Press et al. 1989) with simple bounds on variables. Cases with full vegetation cover and bare soil are are treated separately. Radiometric temperature of homogeneous targets is retrieved in these cases.

Retrieval of soil and foliage temperatures is not performed in the following abnormal situations: a) the difference of surface brightness temperatures for nadir and forward view, $T_{rad}(nadir) - T_{rad}(forward)$ is too large (>7.5K for instance) or b) the difference of surface brightness temperatures is inconsistent with the difference of vegetation fraction covers.

Initial values of soil and foliage temperatures are taken from the approximate solution of equation 5.2 with $B(T) \cong \sigma T^4$, the lower and upper bounds for T_s and T_f are their initial values minus and plus 5K, respectively. If the initial values given by the approximate solution of equation 5.2 are too high for T_s and too low for T_f, T_f is re-initialized by $T_{rad}(forward) - 5K$ and T_s is re-initialized by $T_{rad}(nadir) + 10K$. Finally equation 5.2 is solved to obtain T_s and T_f.

Results and discussions

The procedures described above have been applied to six images of ATSR-2 over Spain (5 images) and USA/SGP'97 (1 image of the South Great Plain, 1997) study areas.

The six ATSR-2 datasets selected by this study cover two sites with distinguished surface properties: five datasets of Spain with sparsely covered surfaces, and one dataset of SGP'97 experimental area with mixed surface types (table 5.3).

Table 5.3 ATSR-2 images used in the study. Image alias is for the convenience for the latter text.

Study Area	Image Date	Image Center Coordinates	Image Alias
South Great Plain, 1997 (USA)	1997.07.01	37.882°N, 94.681°W	SGP970701
Spain	1999.04.13	37.884°N, 4.149°W	SP990413
	1999.06.06	37.891°N, 4.865°W	SP990606
	1999.06.19	37.890°N, 2.701°W	SP990619
	1999.08.28	37.886°N, 2.691°W	SP990828
	1999.09.16	37.885°N, 3.481°W	SP990916

Fractional vegetation cover

Fractional vegetation cover, $F(\theta)$, has been derived by equation 5.3 (referred to as NDVI_method) and equation 5.4 (referred to as OSCAR_method) respectively. Figure 5.2 gives the histograms of $F(\theta)$ from these two methods both at nadir and in the forward zenith view for each image. The distributions $F(\theta)$ estimated by NDVI_method and by OSCAR_method appear quite different. The values of $F(\theta)$ estimated by NDVI_method are systematically larger than the values of $F(\theta)$ obtained from the OSCAR_method both at nadir and in the forward direction over Spain study area, while it is the other way round over SGP97 study area (figure 5.3). Table 5.4 gives the root mean square difference (RMSD) in estimated $F(\theta)$ between the NDVI_method and the OSCAR_method for the six images listed in table 5.3.

At the current stage, it is difficult to evaluate which method would give more accurate values of $F(\theta)$ without knowing precisely the surface characteristics in a pixel. The NDVI_method (equation 5.3) is semi-empirical, may not be adequate to the land surface where no bare soil (or no fully vegetated) patches corresponding to the minimum (or maximum) value of NDVI occur. The OSCAR_method has a robust physical basis. The regression coefficients determined with the OSCAR_method (equation 5.4), however, are generated based on vegetation with green leaves, which may not be appropriate to vegetation with yellow

leaves, likely to occur in most of the area in Spain, especially in the season with a large fraction of dry yellow vegetation. The regression coefficients might have been better representative if they had been produced from a specific data base designed to be closer to the actual situation.

Table 5.4 The RMSD of the difference between $F(\theta)$ estimated by NDVI_method (equation (3)) and that by OSCAR_method (equation (4)) for nadir and forward views.

Images	RMSD of F(nadir) (%)	RMSD of F(forward) (%)
SP990413	6.3	9.1
SP990606	5.5	6.7
SP990619	5.9	6.6
SP990828	7.5	7.9
SP990916	6.9	7.2
SGP970701	9.7	10.7

Soil and foliage temperature

Soil and foliage component temperatures are derived from equation 5.2 with vegetation cover, $F(\theta)$, estimated using both equations 5.3 and 5.4 for comparison. Effective soil and foliage emissivity are needed to solve T_f and T_s from equation 5.2. According to Li et al. (2001a), these values are simply taken as $\varepsilon_s = 0.97$ and $\varepsilon_f = 0.99$. Figure 5.4 shows the histograms of T_f and T_s retrieved with different methods to estimate vegetation cover (equations 5.3 and 5.4).

Large differences exist both in the retrieved T_f and in T_s when $F(\theta)$ are determined using NDVI_method and OSCAR_method respectively (figure 5.5). The biases are significant for retrieval of T_f in Spain study area (figure 5.5a). Table 5.5 gives the RMSD of retrieved T_f (and T_s) using different methods to estimate $F(\theta)$.

As discussed by Li et al. (2001a), the inversion model such as equation 5.1 is sensitive to the estimate of fractional vegetation cover. The sensitivity of T_f and T_s to $F(\theta)$ can be expressed as respectively

$$\left|\frac{\partial T_f}{\partial F(nadir)}\right| = \left|(T_s - T_f)\cdot\frac{F(forward)-1}{F(forward)-F(nadir)}\right| \quad (5.9a)$$

$$\left|\frac{\partial T_f}{\partial F(forward)}\right| = \left|(T_s - T_f)\cdot\frac{1-F(nadir)}{F(forward)-F(nadir)}\right| \quad (5.9b)$$

$$\left|\frac{\partial T_s}{\partial F(nadir)}\right| = \left|(T_s - T_f)\cdot\frac{F(forward)}{F(forward)-F(nadir)}\right| \quad (5.9c)$$

$$\left|\frac{\partial T_s}{\partial F(forward)}\right| = \left|(T_s - T_f)\cdot\frac{-F(nadir)}{F(forward)-F(nadir)}\right| \quad (5.9d)$$

Therefore, under a certain difference of $F(\theta)$ at nadir and in the forward view, the smaller the values of $F(forward)$ (or $F(nadir)$), the larger are errors of T_f due to the errors of $F(nadir)$ (or $F(forward)$) according to equation 5.9a and equation 5.9b. That is to say, at lower fractional vegetation cover, larger errors may result in T_f retrieval. Whereas, at higher fractional vegetation cover, larger errors may occur in T_s retrieval according to equation 5.9c and equation 5.9d. Since the Spain study area has lower $F(\theta)$ values, i.e. lower than 20% exist in most of the area, retrieval of T_f is thus more sensitive to the error on $F(\theta)$. The case in SGP97 area seems to be more complicated.

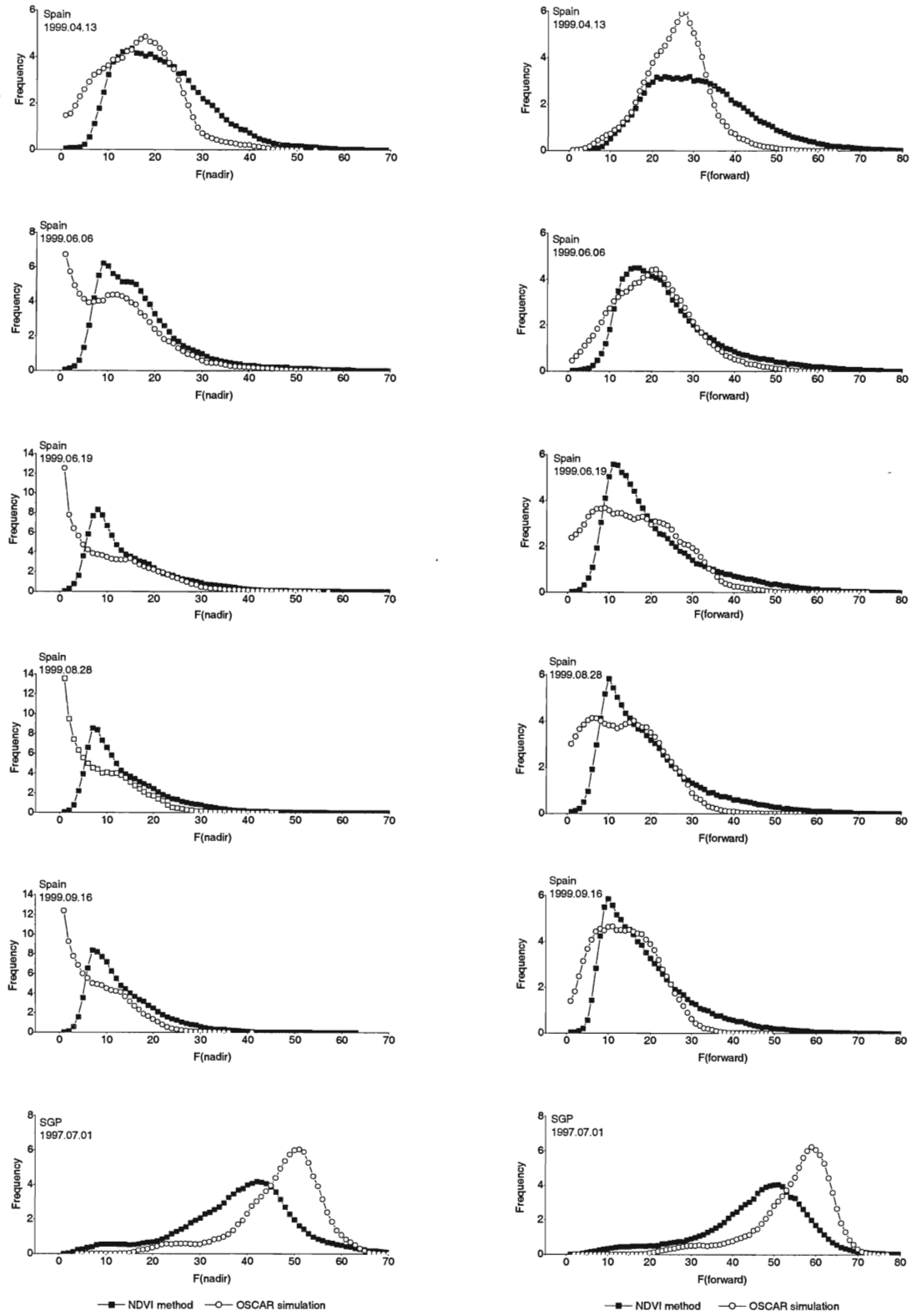

Fig. 5.2: Histograms of fractional vegetation cover estimated using NDVI_method and OSCAR_method for six studied images: (a) for nadir view; (b) for forward view .

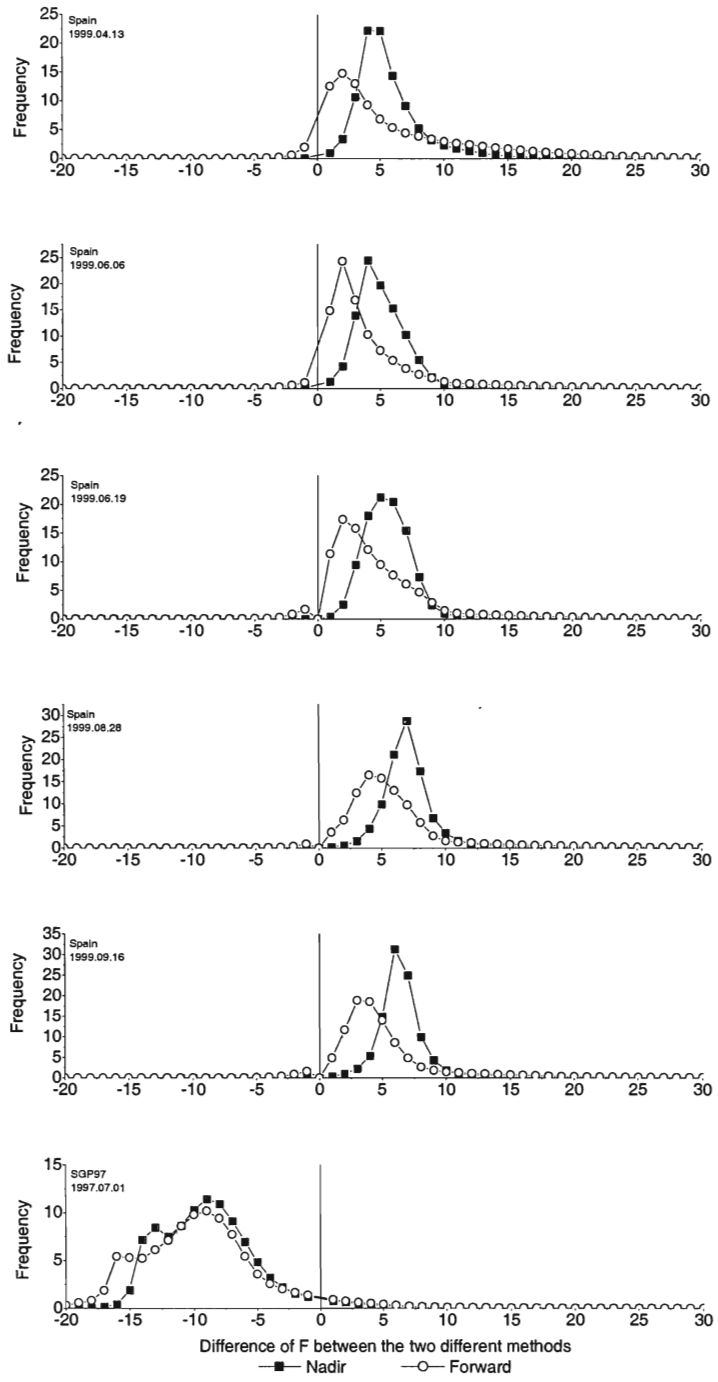

Fig. 5.3 Histograms of the difference between $F(\theta)$ estimated by NDVI_method (Eq. 5.3) and that by OSCAR_method (Eq. 5.4) for nadir and forward views.

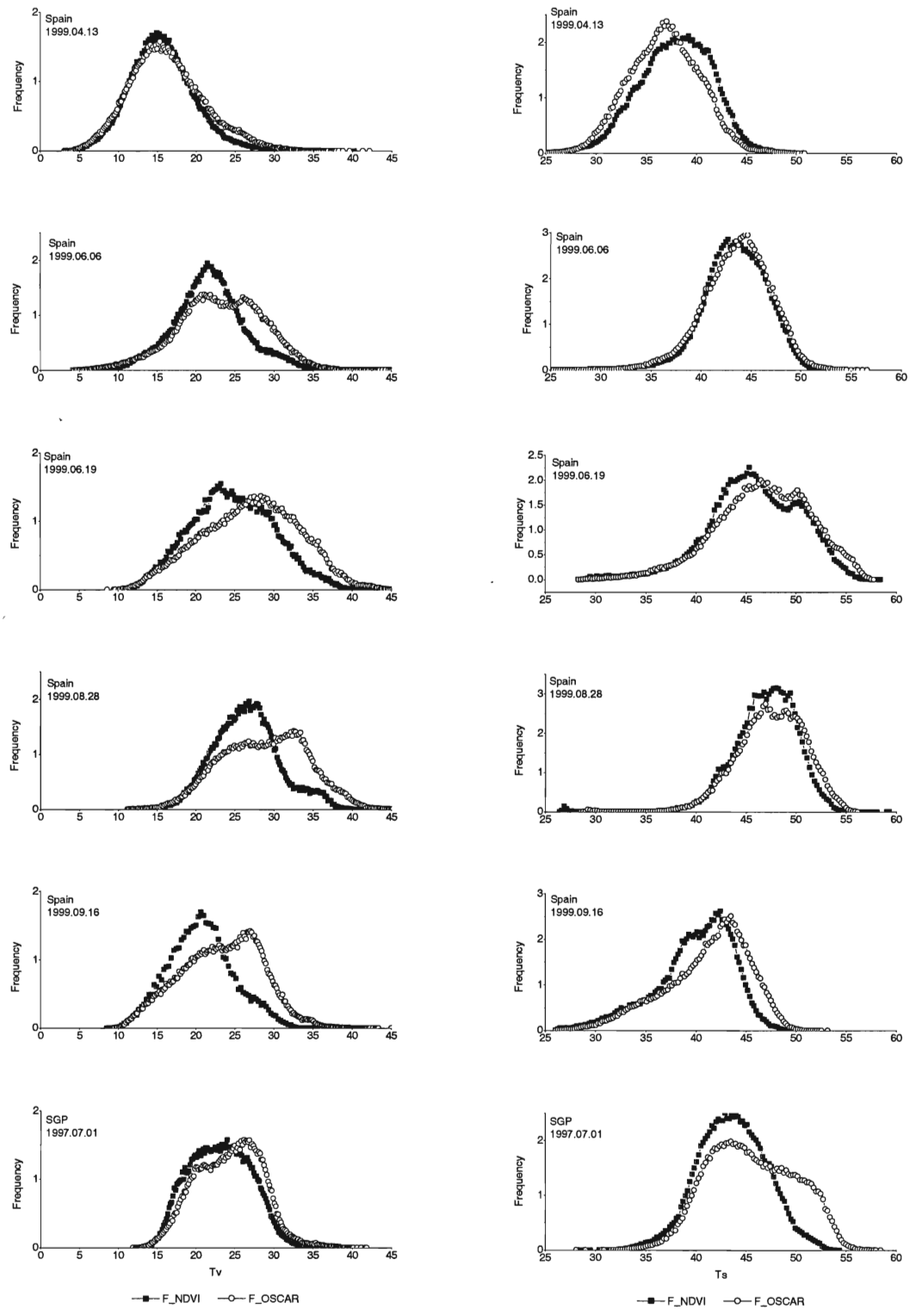

Fig. 5.4 Histograms of (a) T_f and (b) T_s over each study areas. F_NDVI denotes $F(\theta)$ estimated by NDVI_method; while F_OSCAR means $F(\theta)$ estimated by OSCAR_method.

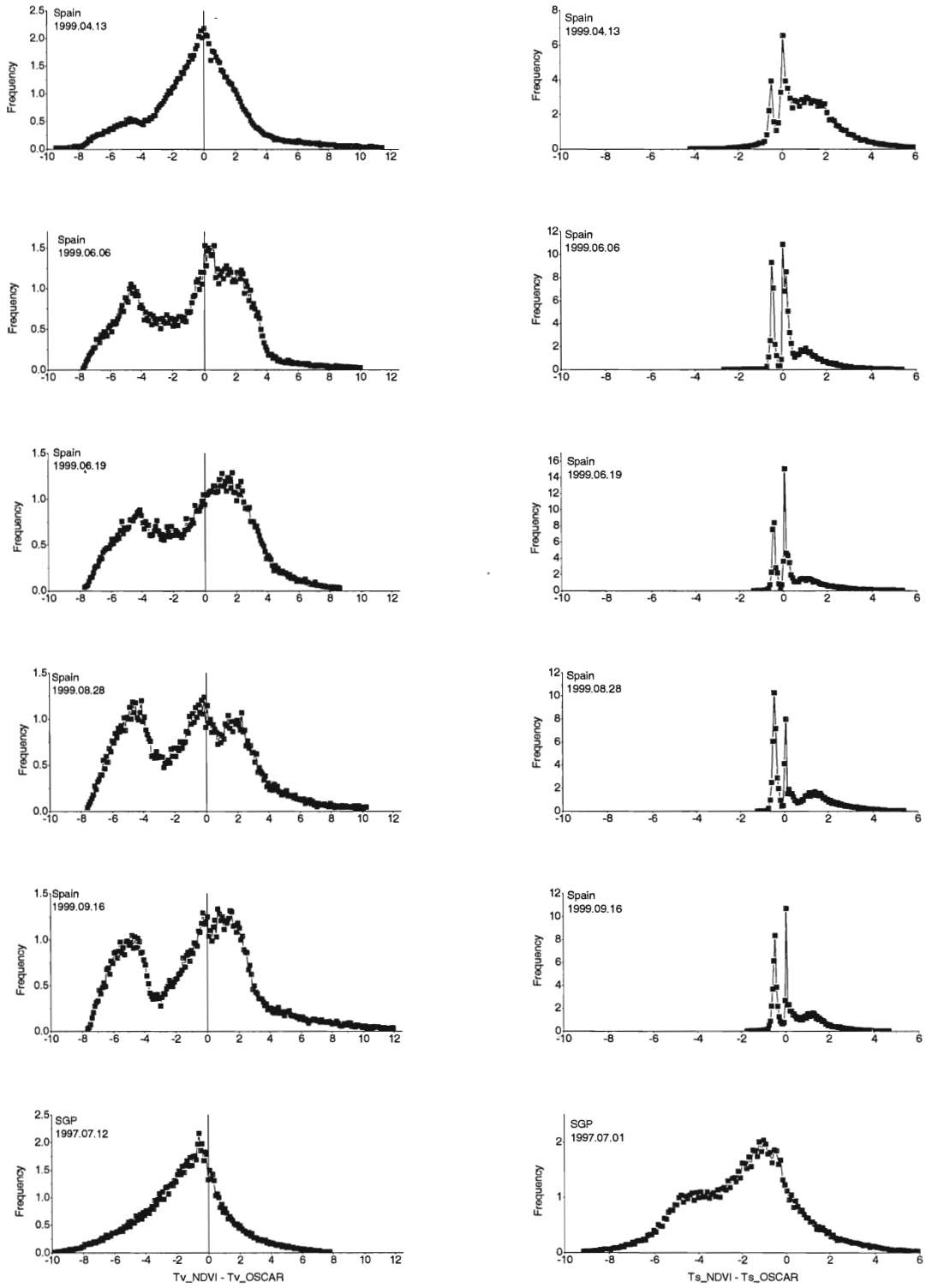

Fig. 5.5 Histograms of the difference of (a) T_f and (b) T_s between using NDVI_method and the OSCAR_method to determine $F(\theta)$.

Table 5.5 The RMSD of retrieved T_f and T_s respectively when using NDVI_method and OSCAR_method to estimate $F(\theta)$.

Images	RMSD of T_f (K)	RMSD of T_s (K)
SP990413	3.23	3.23
SP990606	3.45	2.18
SP990619	3.47	2.80
SP990828	3.76	2.91
SP990916	3.87	2.98
SGP970701	3.11	3.11

Averages of T_f and T_s over NWP model grid

We have previously explored (van den Hurk et al 2001) the application of the component temperatures as inputs of numerical weather prediction (NWP) models such as the one developed at European Center for Medium-range Weather Forecast (ECMWF), so that such models can be improved by taking into account grid heterogeneity of land surface. Grid averaged values of T_f and T_s are needed to meet such requirement.

Grid averaged values from the two methods have been analyzed by averaging $F(\theta)$, T_f and T_s over each grid ($25km \times 25km$) of the NWP model in the Spain study area. Again, $F(\theta)$ derived from NDVI empirical formulation is larger than the one from the simulation method, OSCAR_method (figure 5.6). However, it is worth to note that the retrievals of T_f and T_s show quite similar values when using either one of the two methods to derive $F(\theta)$ (figure 5.7). The values of RMSD for $F(\theta)$, T_f and T_s are given in table 5.6.

Table 5.6 The RMSD of $F(nadir)$, T_f and T_s over NWP grid due to different methods (equations 5.3 and 5.4) used to estimate $F(\theta)$.

Imagery	RMSD of F(nadir) (%)	RMSD of T_f (K)	RMSD of T_s (K)
SP19990413	6.0	1.51	1.25
SP19990606	5.3	1.91	1.18
SP19990619	5.7	2.23	1.58
SP19990828	6.8	2.60	1.59
SP19990916	6.5	3.00	1.70

Compared with the values of RMSD of $F(\theta)$, T_f and T_s at pixel level, the values of RMSD of $F(\theta)$, T_f and T_s averaged over a NWP grid become smaller. The errors on T_f and T_s over a grid are reduced as much as about 1.5 – 2 times (see tables 5.5 and 5.6). This implies that uncertainty in determination of fractional vegetation cover in ATSR-2 pixel scale may not affect too much the statistics of T_f and T_s over a grid of NWP. Although the accuracy of the retrieved T_f and T_s still need to be investigated, the use of the component temperatures in NWP model is quite promising. A preliminary case study has been done by employing these two component temperatures in a newly developed multi-component land surface parameterization scheme (van den Hurk et al. 2001), in which improvements in the estimation of surface energy balance have been obtained.

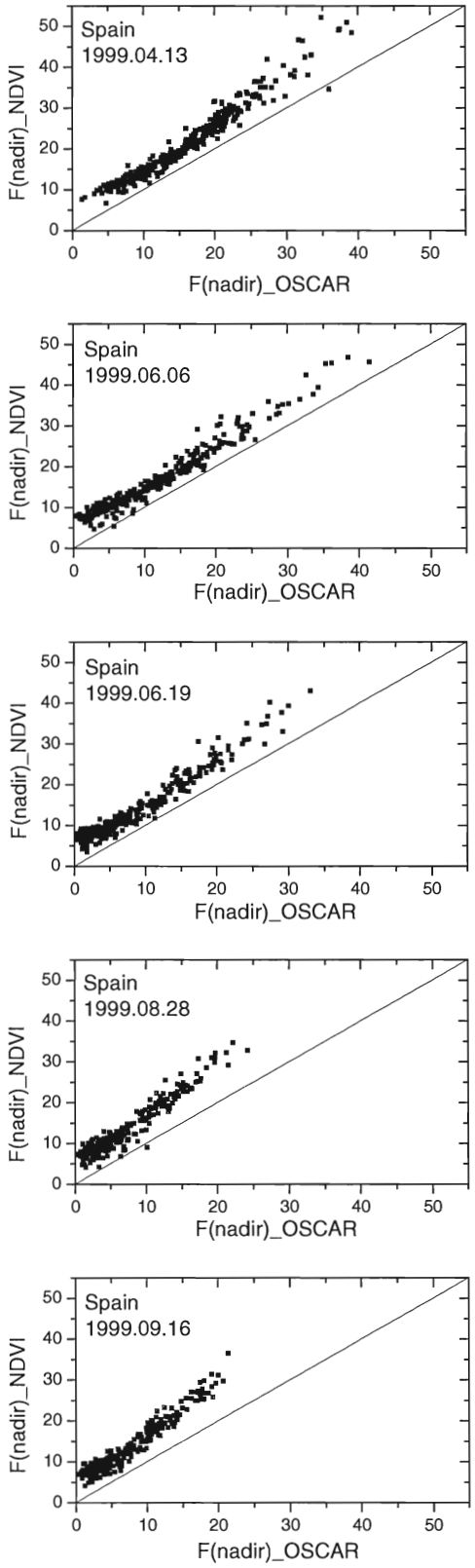

Fig. 5.6 Comparison of the average of fractional vegetation cover at nadir derived from NDVI empirical method (Eq.5.3) and the OSCAR simulation method (eq.5.4) over NWP sub-grid. $F(nadir)\_NDVI$: F(nadir) derived using NDVI empirical method; $F(nadir)\_OSCAR$: F(nadir) derived using the OSCAR model simulation method.

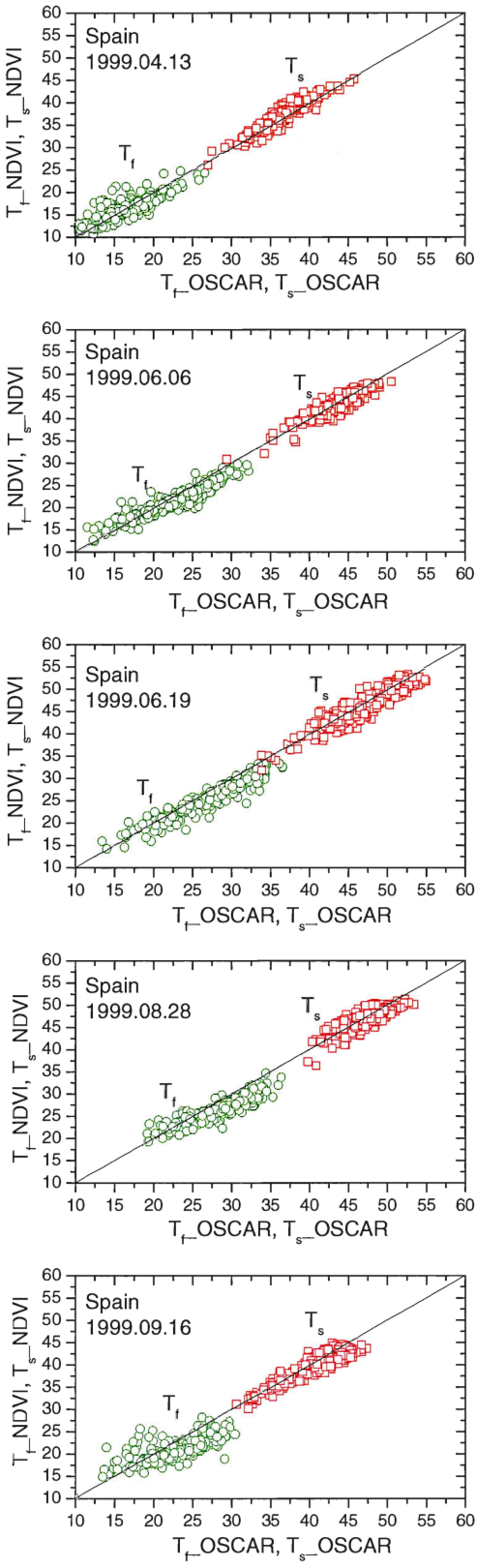

Fig. 5.7 Comparison of the average of T_f (T_s) over NWP sub-grid obtained using different methods to derive fractional vegetation cover. T_f_NDVI (T_s_NDVI): $F(\theta)$ from NDVI semi-empirical formula; T_f_OSCAR (T_s_OSCAR): $F(\theta)$ from the OSCAR model simulation method.

Validation

The validation of the retrieved component temperatures is challenging due to the difficulty of obtaining observations of temperatures of soil and foliage in situ at ATSR-2 spatial resolution. Some authors have found through experiments that leaves of most crops were essentially close to air temperature (Miller and Saunder 1923, Ehrler 1973). Following these conclusions, the results are roughly validated by comparing the derived T_f with the air temperature in our study (figure 5.8). In Spain area, several synops stations which are located in the images are selected as the reference sites. In SGP'97 area, two sites (CF01 and CF02) are chosen as the reference sites. The air temperatures at synops stations were measured at 2 meters height, while at the two SGP'97 experimental sites air temperature was measured at 0.96 and 1.96 meters height at site CF01 and at 3 meters height at site CF02, respectively. The reference air temperature for SGP'97 area is taken as the mean between two measurements before and after ATSR-2 passing time over the two reference sites. In figure 5.8, the values of retrieved T_f and T_s are the average over 5×5 pixels around each reference site. The error bars indicate the standard deviations of T_f averaged over 5×5 pixels.

As shown in figure 5.8, the values of T_f are in agreement with the air temperatures at most of the reference sites. Discrepancy is larger at few sites. It is not surprising to observe some differences between T_f and air temperature. Several environmental influence factors, such as radiation, convection and transpiration, affect T_f. Larger differences between foliage and air temperature were noted both from measurements and modelling results (see Jackson 1982).

Measurements of directional TIR and component temperatures at higher spatial resolution are needed to accomplish more accurate validation of the retrieved component temperatures.

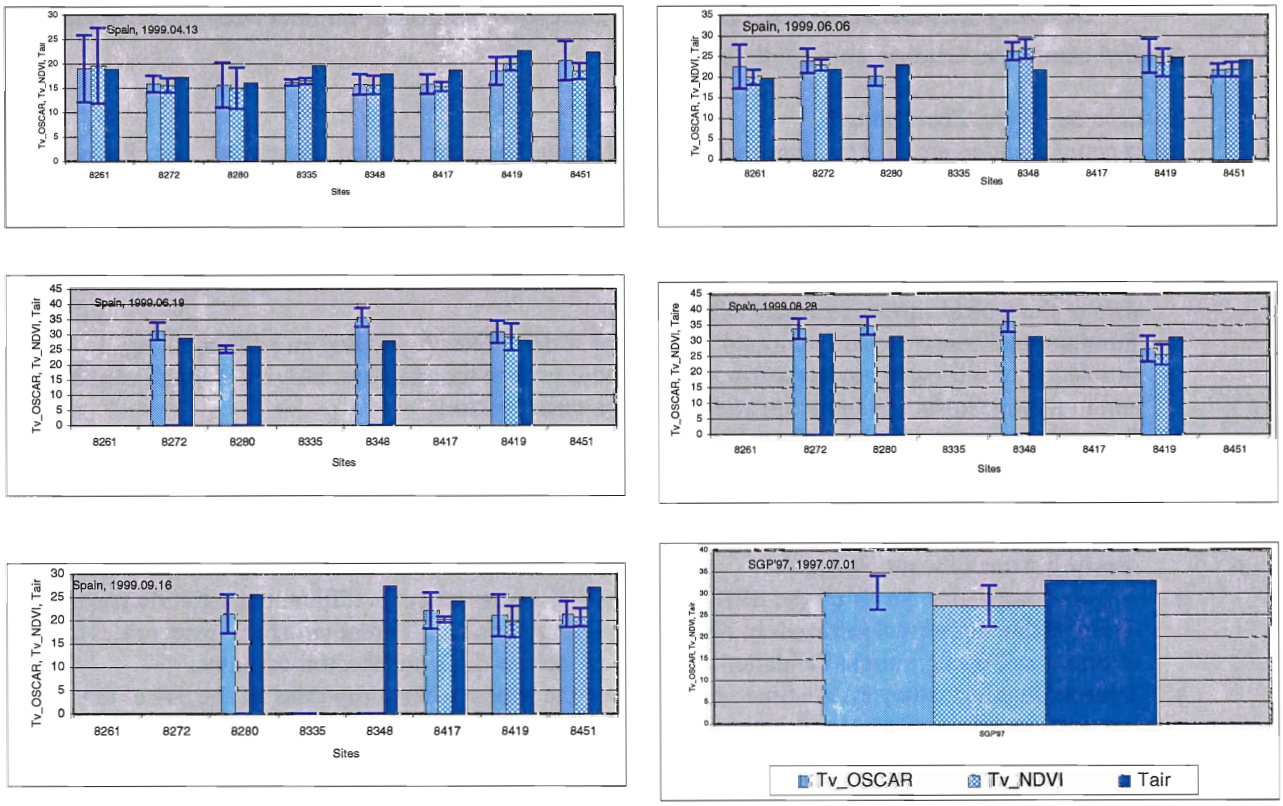

Fig. 5.8 Comparison between foliage temperatures and the air temperatures at reference sites in Spain and SGP'97 study area. The numbers in X-axis denoted the sites in Spain area are the WMO meteorology station numbers. The error bars indicate the standard deviations of T_f averaged over 5×5 pixels. The absences of T_f denote available pixels with derived T_f values are less than 5 pixels which is considered less presentation of 5×5 pixels window.

Conclusions

This study developed a practical algorithm to derive component temperatures of soil and foliage using multi-spectral and dual-view angle measurements made by ATSR-2. The results appear to be encouraging. The fractional vegetation cover is a crucial parameter in this algorithm. Our analysis does show, however, that the impact on the retrieval of soil and foliage temperature is limited. For the purpose of applying the derived component temperatures in a NWP model, the uncertainty in the estimation of fractional vegetation cover becomes a minor problem. The averages of soil and foliage over a grid of the NWP model show that similar values of component temperatures are obtained even though the difference in fractional vegetation cover obtained with two different methods is significant.

Validation was very preliminary made by comparing T_f to air temperature. In most cases, T_f was comparable to air temperatures which implies that our simple linear inversion model can be applied to separate the two components temperatures based on the use of bi-angular TIR measurements. Angular measurements at higher spatial resolution are necessary to obtain a more accurate validation of our methods.

In future work, validation based on field measurements of component temperatures will be necessary. To this end, data collected from a recent field campaign in Shunyi, China will be valuable. During this field campaign, thermal imaging camera was deployed in-situ making continuous measurements of multi-angle measurements. Upon proper processing, these data can be used to validate the algorithm developed in this study.

Contribution to field experiment: A brief introduction for Comprehensive Remote Sensing Experiment With the aid of Satellite-Airborne-In situ Measurements

(Shunyi campaign, October 2000 --- October 2001)

Zhongbo Su, Li Jia, Zhao-Liang Li

Based on information provided by Xiaowen Li (Bejing Normal University/Boston University), Prof. Renhua Zhang, Prof. Qinhuo Liu, Dr. Qiang Liu (Chinese Academy of Sciences)

The Objectives of the Shunyi campaign were

1. Acquire, at different times and different scales, the multispectral and multi-angle remote sensing data of the typical surface features- winter wheat.
2. Fundamental researches on temporal and spatial scales effects (upscaling and downscaling problems) of retrieving surface attributes – albedo; surface temperature, LAI, chlorophyll content, soil moisture, surface evaporation and vegetation transpiration.
3. Spectral properties: Study on the relationships between the spectral properties of winter wheat in different soil background and in different growing periods and the physiochemical and biochemical components (water content in the canopy, chlorophyll content, nitrogen content etc); Selection of optimum channels and establishment of quantitative model for monitoring of the drought and the growing states of winter wheat.
4. Angular properties: Study on the BRDF properties of winter wheat in different spectral domains (from visible to thermal infrared) in different growing periods, different structural parameters and different soil backgrounds; Validation of BRDF models in different spectral domains.
5. Time scale effect: study on the time scale effect of the winter wheat properties by the use of the temporal variation of winter wheat parameters in different growing periods (canopy structural parameters, canopy temperature, spectral characteristics and evapotranspiration)
6. Spatial scale effect: study on the spatial scale effect of remote sensed canopy properties (albedo, temperature, sensible and latent fluxes etc) through the use of remote sensed data in different spectral domains and at different spatial resolutions
7. Validation of remote sensing models and the retrieving accuracy of different parameters.
8. Study on the water-heat transfer model in the farm ecosystem

The planned observations were:

1) Observation Sites
   a) Satellite remote sensing experiment site: North-China Plain
   b) Airborne remote sensing experiment site: ShunYi (116°26'E-117°E, 40°N-40°21'N)
   c) In-situ (field) remote sensing experiment sites: YuCheng, LuanCheng and ShunYi

2) Observation periods:
   a) *Intensive Observation Period (4/05/2001-4/25/2001)* Besides the increase of the observation density with respect to the observation taken in the normal observation period, high spectral and multispectral and multi-angle airborne observations will be conducted at ShunYi site near Beijing. The farmlands in ShunYi experiment site is monitored by scientists so that the winter wheat is planted in different ways (different row distances, different seeding densities) and is growing under different water and fertilizer supplies.
   b) *Normal Observation Period (3/20/2001-4/30/2001)* In addition to the increase of the observation density with respect to the observation taken in the extended observation period, satellite data at coarse spatial resolution such as AVHRR, MODIS, FY-2, ATSR-2 will be acquired over North-China Plain region and satellite data at high spatial resolution such as TM, SPOT, ASTER, MISR, IKONOS will be acquired over ShunYi site. Solar spectral irradiance, atmospheric profiles and aerosol characteristics will be measured in synchronization with satellite passes. During that period, soil and crop physiochemical parameters, biochemical parameters, biomass and canopy structural parameters, spectral data and BRDF distribution in different spectral domains from visible to thermal infrared will be measured.
   c) *Extended Observation Period (10/01/2000-6/30/2001)* During the whole growing period of winter wheat, traditional meteorological measurements and local scale climate observations in farmlands will be conducted at YuCheng and LuanCheng sites. Meanwhile, water and fertilizer supplies to the experiment farmlands will be recoded. The variation of biomass, structural parameters and others auxiliary data will also be measured.

WP 6: Sensible and latent heat fluxes: Evaluation of the Surface Energy Balance System (SEBS) using ATSR and scintillometer measurements and RACMO PBL variables

Li Jia, Zhongbo Su(1), Bart van den Hurk, Arnold F. Moene and Massimo Menenti

Introduction

The estimation of atmospheric turbulent fluxes at the land surface has long been recognised as the most important process in the determination of the exchanges of energy and mass among hydrosphere, atmosphere and biosphere. Remote sensing is probably the only technique which can provide representative measurements of several relevant physical parameters at scales from a point to a continent. Techniques using remote sensing information to estimate atmospheric turbulent fluxes are therefore essential when dealing with processes that can not be represented only by point measurements.

Methods using remote sensing information to estimate heat exchange between land surface and atmosphere can be broadly put into two categories: to calculate the sensible heat flux first and then to obtain the latent heat flux as the residual of the energy balance equation; or to estimate the relative evaporation by means of an index using a combination equation. Although successful estimations of heat fluxes have been obtained over small-scale horizontal homogeneous surfaces, difficulties remain in estimations for partial canopies which are geometrically and thermally heterogeneous. Classical remote sensing flux algorithms based on surface temperature measurements in combination with spatially constant surface meteorological parameters may be suitable for assessing the surface fluxes on a small scale, but they will fail for larger scales at which the surface meteorological parameters are no longer constant, and the surface geometrical and thermal conditions are neither homogenous nor constant any more. Hence, more advanced algorithms need to be designed for composite terrain at a larger scale with heterogeneous surfaces.

In this contribution the Surface Energy Balance System (SEBS) derived by Su (2001) for the estimation of atmospheric turbulent fluxes using satellite earth observation data are evaluated with measurements of sensible heat fluxes by scintillometry. The input to SEBS are ATSR derived surface physical variables and atmospheric boundary layer variables derived from the mesoscale atmospheric model RACMO. SEBS as proposed here consists of:

- a set of tools for the determination of the land surface physical parameters, such as albedo, emissivity, temperature, vegetation coverage etc. from spectral reflectance and radiance (Su et al., 1999);

- an extended model for the determination of the roughness length for heat transfer of Su et al. (2001); and
- a new formulation for the determination of the evaporative fraction on the basis of energy balance at limiting cases.

In the present set-up, SEBS requires three sets of information as inputs. The first set consists of land surface albedo, emissivity, temperature, fractional vegetation coverage and leaf area index, and the height of the vegetation (or roughness height). When vegetation information is not explicitly available, the Normalized Difference Vegetation Index (NDVI) is used as a surrogate. These inputs can be derived from remote sensing data in conjunction with other information about the concerned surface. The second set includes air pressure, temperature, humidity, and wind speed at a reference height. The reference height is the measurement height for point application and the height of the planetary boundary layer (PBL) for regional application. This data set can also be variables estimated by a large scale meteorological model. The third data set includes downward solar radiation, and downward longwave radiation which can either be directly measurements, model output or parameterization.

Data

Field measurements

Sensible heat flux measurements were made simultaneously using large aperture scintillometer (LAS) in three experimental sites in Spain: Lleida, Tomelloso and Badajoz (see Fig. 6.1 for the locations of sites). At each location a scintillometer was set up with additional global radiation measurements. Measurements used in this study were made on available ATSR passing day during April and September in 1999. Additional data that are necessary for the processing of LAS data were obtained from weather stations in the near surroundings.

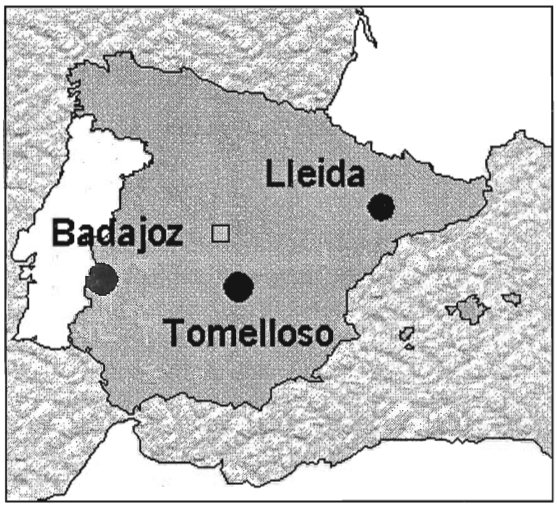

Figure 6.1 Location of scintillometer measurements sites in Spain.

The LAS used at each location was manufactured by the Meteorology and Air Quality Group of Wageningen University. The readers are referred to Su and Jacobs (2001) for the detailed descriptions of measurements.

The three experimental sites are composed of different surface properties ranging from dry area to irrigated area. The summarization of measurements and surface characteristic are given in Table 6.1.

Remote sensing data

Remote sensing data used in this study are acquired by the Along Track Scanning Radiometer (ATSR)-2 on board the European Remote Sensing satellite (ERS). ATSR-2 has four channels in the visible and near infrared domain (0.55μm, 0.65μm, 0.87μm, 1.60μm) and three channels in the thermal infrared domain (3.7μm, 11μm and 12μm) in nadir and forward view angles. Reflectances in four VIS/NIR are used to carry out the atmospheric correction for these channels (Jia et al. 2000), consequently to estimate surface albedo and fractional vegetation cover. Surface brightness temperature is obtained by apply a Split-window

method to the two thermal infrared channels (11μm and 12μm) (Li et al., 2000). The available images and field observations are listed in Table 6.2.

Table 6.1 Summary of characteristics of scintillometer experimental sites in Spain

Site	Transmitter		Receiver		Distance	Surface Characteristics
	Location	Height (m)	Location	Height (m)	(m)	
Tomelloso	39°07.357'N 2°55.314'W	4.56	39°07.653'N 2°55.951'W	4.15	1070	Dry vineyard
Lleida	41°32.644'N 0°51.644'E	39	41°34.962'N 0°52.444'E	45	4440	Small scale irrigation area with fruit trees, alfalfa
Badajoz	38°55.697'N 6°36.590'W	68	38°56.298'N 6°40.141'W	56	5250	Large scale irrigation area with wheat, corn, alfalfa, lettuce, olives, beans, tomatoes.

Methodology

Surface Energy Balance System (SEBS)

The Surface Energy Balance System (SEBS) was proposed by Su (2001) for the estimation of atmospheric turbulent fluxes and surface evaporation using satellite earth observation data in the visible, near infra-red, and thermal infrared regions.

Table 6.2. ATSR images and scintillometer observations used in the study. The numbers in the first column shows the images' name by dates(YYMMDD). Under each site, YES denotes both images and scintillometer observation are available and used for sensible heat flux calculation.

Images	Tomelloso	Lleida	Badajoz
990413	Yes		
990606	Yes		
990619	Yes		
990715		Yes	
990721		Yes	
990730			Yes
990815			Yes
990821			Yes
990828	Yes		
990916	Yes		
990929		Yes	

SEBS consists of the following main concepts to carry out the estimation of heat fluxes from the surface:

- A model for the determination of the roughness length for heat transfer (Su et al. 2001);

- The BAS (Bulk Atmospheric Similarity) theory for determination of friction velocity, sensible heat flux and the Obukhov stability length (Brutsaert, 1999);
- The SEBI (Surface Energy Balance Index) concept for determination of evaporative fraction (Menenti & Choudhury, 1993).

The energy balance between the land surface and the atmosphere is usually expressed as the partitioning of available energy between the sensible and latent heat fluxes

$$R_n - G = H + \lambda E \tag{6.1}$$

where R_n is the net radiation arrived at the surface, G is the heat conduction into the soil, H is the sensible heat flux, λE is the latent heat flux.

The ratio of actual (λE) to maximum (λE_p) latent heat flux, i.e. the relative evaporation is related to the actual, minimum and maximum difference between surface and air temperature at the reference height as:

$$\frac{\lambda E}{\lambda E_p} = 1 - \frac{\dfrac{(T_0 - T_a)}{r_e} - \dfrac{(T_0 - T_a)_l}{(r_e)_l}}{\dfrac{(T_0 - T_a)_u}{(r_e)_u} - \dfrac{(T_0 - T_a)_l}{(r_e)_l}} = 1 - SEBI \tag{6.2}$$

where T_0 (K) is the surface temperature; T_a (K) is the air temperature at reference height; r_e (s m^{-1}) is the external resistance, namely aerodynamic resistance for heat transfer, and is expressed as

$$r_e = \frac{1}{ku_*}\left[\ln\left(\frac{z-d}{z_{0h}}\right) - \psi_h\left(\frac{z-d}{L}\right) + \psi_h\left(\frac{z_{0h}}{L}\right)\right] \tag{6.3}$$

where k = 0.4 is von Karman's constant, u_* (m s^{-1}) is the friction velocity, d (m) is the zero plane displacement height, z_{0h} (m) is the roughness height for heat transfer, ψ_m and ψ_h are the stability correction functions for momentum and sensible heat transfer respectively, L is the Monin-Obukhov length defined as

$$L = -\frac{\rho_a c_p u_*^3 \theta_v}{kgH} \tag{6.4}$$

where ρ_a is the air density (kg m^{-3}); c_p is the specific heat of air at constant pressure (=1005 J kg^{-1} K^{-1}); θ_v is the potential virtual temperature (K); g is the acceleration due to gravity (m s^{-2}).

The evaporative fraction is defined as

$$\Lambda = \frac{\lambda E}{R_n - G} = (1 - SEBI)\frac{\lambda E_w}{R_n - G} \tag{6.5}$$

Combining Eqs. (6.1), (6.2) and (6.5), surface sensible and latent heat fluxes can be obtained:

$$\lambda E = (1 - SEBI)\lambda E_w \tag{6.6}$$

and

$$H = (1 - \Lambda)(R_n - G) \tag{6.7}$$

To estimate heat transfer over regional scale, BAS function (Brutsaert, 1999) should be used to obtain the stability correction functions ψ_m and ψ_h (see Su et al, 2001 for details).

Determination of PBL variables

Planet Boundary Layer (PBL) is considered as a suitable reference level (Brutsaert and Sugita, 1992) to estimate regional heat flux. The interdependence of horizontal and vertical length scales in relation with PBL fluxes was addressed by e.g. Finnigan et al. (1990) who related horizontal, X, to vertical length scales as:

$$X = \frac{u}{u_*} h_i \tag{6.8}$$

where h_i is the blending height of boundary layer under neutral conditions. With the magnitude of u/u_* ~10-100, the ratio of vertical scale to horizontal scale is about $\frac{1}{100} \sim \frac{1}{10}$.

The radiosounding measurement in meteorology stations is the possible way to obtain blending height and wind speed, potential temperature and humidity at this height. However, the distribution density of meteorology station over the world is usually not as enough as needed in regional scale. In this study, these variables at blending height are produced by RACMO model with $25km \times 25km$ resolution. According to Eq. (6.8), such horizontal scale is suitable to the blending height in most boundary layer conditions.

Determination of Surface parameters

Surface albedo

Surface albedo α has been derived from surface reflectances $\rho_i(\theta_s, \Delta\phi)$ using the stepwise multiple linear regression

$$\alpha = a_0(\theta_s) + \sum_{i=1}^{n} [a_i(nadir, \theta_s)\rho_i(nadir, \theta_s, \Delta\phi)] + \sum_{i=1}^{n} [a_i(forward, \theta_s)\rho_i(forward, \theta_s, \Delta\phi)] \tag{6.9}$$

where n is the number of channels used in the range of visible to SWIR channels, θ_s is solar zenith angle, $\Delta\phi$ is the relative azimuth angle between sun and satellite direction. The coefficients a_i in equation (6.9) were derived by applying OSCAR model to the ensemble of canopy and atmospheric conditions (Verhoef, 2001, private communication; also see Jia et al 2001 for details) corresponding to the ATSR-2 observations. Reflectances in the four optical bands (0.55μm, 0.65μm, 0.87μm and 1.6μm) were simulated for nadir view of ATSR observations. The relative azimuth angle was roughly estimated to be equal to 120 degrees. For all combinations of the simulated conditions (Verhof, 2001) the reflectance was computed in the above four ATSR-2 bands in the nadir view angle at the surface level. Table 6.3 gives the values of regression coefficients in the different solar zenith angles (θ_s) and the coefficients of determination R^2 which is the measure of the quality of parameter retrieval. The coefficients in table 6.3 are then interpolated to each ATSR-2 pixel according to the solar zenith angle for each pixel.

Table 6.3 The regression coefficients in the stepwise multiple linear regression (Eq. (6.9)) generated by OSCAR model at different solar zenith angle (θ_s). R^2 is the square of correlation coefficients.

θ_s (°)	a_0	a_1 (n)	a_2 (n)	a_3 (n)	a_4 (n)	a_1 (f)	a_2 (f)	a_3 (f)	a_4 (f)	R^2
15	0.0074	-0.16	-0.07	0.03	0.28	0.31	0.23	0.37	-0.09	99.8
30	0.0144	0.09	-0.25	-0.13	0.59	0.04	0.44	0.55	-0.45	99.7
45	0.0169	0.15	0.07	-0.24	0.69	-0.03	0.12	0.68	-0.57	99.6
60	0.0096	0.01	0.74	-0.14	0.40	0.11	-0.63	0.57	-0.20	99.4
75	-0.0030	-0.10	1.19	0.12	-0.05	0.23	-1.18	0.29	0.36	99.4

Atmospheric corrections were carried out to obtain reflectances at the bottom of atmosphere (BOA) from reflectances at the top of atmosphere (TOA) measured by ATSR in VIS/NIR channels (Jia, et al., 2001).

Surface vegetation fraction cover, f_c

Vegetation fraction cover is estimated using a semi-empirical formulation (Baret et al., 1995)

$$f_c = 1 - \left(\frac{NDVI - NDVI_{\max}}{NDVI_{\min} - NDVI_{\max}} \right)^K \tag{6.10}$$

with

$$NDVI = \frac{\rho_{nir} - \rho_{vis}}{\rho_{nir} + \rho_{vis}} \tag{6.11}$$

where $NDVI_{\max}$ and $NDVI_{\min}$ are the vegetation index after atmospheric corrections for infinite leaf area index (LAI) and for the bare soil ($LAI = 0$), respectively; ρ_{vis} and ρ_{nir} are the BOA reflectances in visible and near-infrared channels.

Surface roughness parameters, z_{0m} and z_{0h}

Several models have been developed to estimate roughness length for momentum with consideration of the canopy structures (Raupach, 1992, 1994; Massman, 1997). When applying these physically detailed models to regional scale, difficulties are encountered due to lack of the information needed by the models. No further investigations have been carried out in this aspect in this study. Based on studies from different researchers (Hatfield, 1988; Asrar et al., 1992), a relationship between z_{0m} and $NDVI$ maybe expected so that measurements made by satellites can be used for regional estimation of z_{0m}.

The following empirical relationship between z_{0m} and $NDVI$ derived in the same area by Bastiaanssen (1995) is used to estimate surface roughness length for momentum transfer

$$z_{0m} = \exp(C_1 + C_2 \cdot NDVI) \tag{6.12}$$

where C_1 and C_2 are empirical coefficients which are study area dependent. Following Bastiaanssen's (1995) study, $C_1 = -5.5$ and $C_2 = 5.8$ for Tomelloso and $C_1 = -5.2$ and $C_2 = 5.3$ for Barrax. The major difference between these two curves is that slightly higher value of z_{0m} is obtained in Tomelloso site than in Barrax site with the same value of $NDVI$ in the range of higher $NDVI$ ($NDVI > 0.7$ for instance) (see Fig. 6.2).

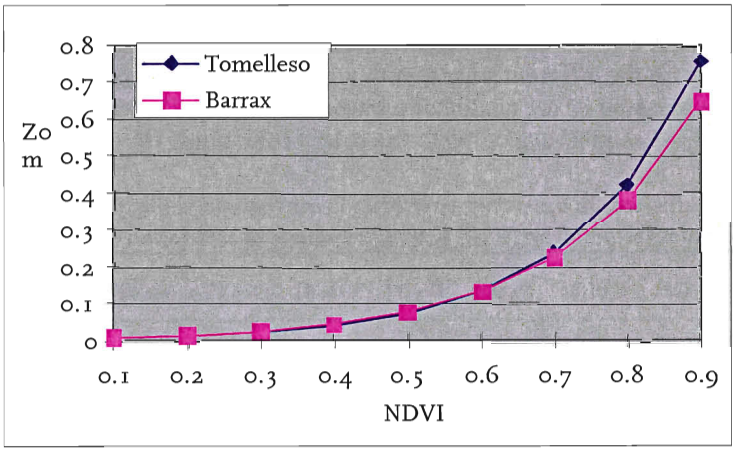

Fig. 6.2 The relationship between z_{0m} and $NDVI$ in Tomelloso and Barrax site, respectively.

A new physically based model for roughness length for heat transfer has been developed by Su et al (2001). In their model, the z_{0h} in terms of kB^{-1} ($= \ln(z_{0h}/z_{0m})$) is expressed as the function of surface condition and the aerodynamic variables

$$kB^{-1} = \frac{kC_d}{4C_t \frac{u_*}{u(h)}\left(1 - e^{-n/2}\right)} f_c^2 + \frac{k \cdot u_*/u(h) \cdot z_{0m}/h}{C_t^*} f_c^2 f_s^2 + kB_s^{-1} f_s^2 \tag{6.13}$$

where C_d is the drag coefficient of the foliage taken as 0.2, C_t is the heat transfer coefficient of the leaf ranging in $0.005N \le C_t \le 0.075N$ (N is number of sides of a leaf to participate in heat exchange), $u(h)$

is the horizontal wind speed at the canopy height, n is the wind speed profile extinction within the canopy, f_s is the fractional cover for soil ($=1-f_c$), C_t^* the heat transfer coefficient of the soil and is given by $C_t^* = \mathrm{Pr}^{-2/3}\,\mathrm{Re}_*^{-1/2}$, where Pr is the Prandtl number (0.71, Massman 1999) and the roughness Reynolds number $\mathrm{Re}_* = h_s u_* / \nu$, with h_s the roughness height of the soil, kB_s^{-1} is the value for bare soil surface.

The three terms in the right hand side of Eq. (6.13) represent the contributions of canopy only, canopy-soil interaction and soil only, respectively. Eq. (6.13) reduces to limiting cases of canopy only for $f_c = 1$ and soil surface only for $f_s = 1$. The reader is encouraged to refer to Su et al. (2001) for the details of this model.

Dual-source model concept

Normally, the land surface consists of vegetation and soil components which react to the atmosphere individually. Neglecting the inter reaction between these two components and assuming they are the two parallel sources for heat transfer, Eqs. (6.2)-(6.6) still holds for each vegetation-atmosphere and soil-atmosphere systems respectively. Eq. (6.13) can be rewritten for each component surface as well. The vegetation and soil temperatures are inverted using a practical algorithm (Jia et al., 2001). The calculations based on this simplified dual-source concept are also dealt in the following section in this report.

Results

Comparison of roughness between SEBS and RACMO

The surface roughness estimated by Eq. (6.12) is more local representative comparing to the one used in RACMO model. This leads the values of z_{0m} in SEBS being much smaller than in those used in RACMO model (Fig. 6.3).

z_{0h} in terms of kB^{-1} has been calculated by Eq. (6.13) in each pixel using ATSR measurements. Comparing to the values obtained by assimilation of land component surface temperatures using RACMO (van den Hurk et al., 2001), the values of kB^{-1} derived by Eq. (6.13) are much smaller and have less variability (Fig. 6.4). To utilize the satellite measurements into GCMs, it is necessary to investigate the relationship by which the information at small scale can be properly transferred to the one needed in climate model.

Sensible heat flux

Sensible heat flux was calculated by Eq. (6.7) (referred to as single-source concept) for ATSR passing time on each day listed in table 6.2. The pixels along the path length of scintillometer observation in each experimental site are picked up, over which the mean and standard deviation of H are calculated (Table 6.4). The results from SEBS are quite comparable with the measurements made by scintillometer with RMSD 16.1, 40.4 and 18.3 W m^{-2} in Tomelloso with dry vineyard surface, Lleida with small scale irrigation area with fruit trees, alfalfa and Badajos with large scale irrigation area with various crops respectively (Fig. 6.5). The total RMSD is about 25 W m^{-2}. It is not a surprise in Tomelloso site to have the smallest RMSD mostly because that the empirical formula for estimating z_{0m} (Eq. (6.12)) and the coefficients used were developed in this area.

The results based on the parallel dual-source concept are also listed in table 6.4. The component temperatures are not available in the all pixels because the inversion technique is limited by the surface conditions and the directional signature captured by the satellite. This results in that the component temperatures are not available in some ATSR pixels so that there are no estimations of heat flux by means of dual-source concept over these pixels. The results from the dual-source concept show smaller than observations in Lleida and larger than observation in Badajoz systematically. A more detailed study needs to be done to investigate the reasons.

The statistics of H estimated by SEBS are also carried out by means of picking up all the ATSR pixels over the RACMO grid ($25km \times 25km$) which is located in the corresponding site. The values in the last column of table 4 are the results from first guess RACMO estimations. The results from RACMO model show the trend of larger values either than observations or the estimations by SEBS in most cases. The RMSD between SEBS and RACMO model estimations is as large as up to about 75 W m^{-2} (Fig. 6.6). More validation material on RACMO is presented in Workpackage 8.

Discussions and conclusions

SEBS has been applied to ATSR data sets of three different surfaces and the prediction of sensible heat flux is compared with sentillometer measurements. The necessary input data were derived from ATSR data and RACMO meteorological fields and applied to SEBS. Some specific conclusions are as follows:

- The results from SEBS are comparable with the measurements made by scintillometer with RMSD 16.1, 40.4 and 18.3 W m^{-2} in Tomelloso with dry vineyard surface, Lleida with small scale irrigation area with fruit trees, alfalfa and Badajos with large scale irrigation area with various crops respectively. The total RMSD is about 25 W m^{-2}.
- The results from the dual-source concept show smaller than observations in Lleida and larger than observation in Badajoz systematically. At present, it has not been possible to figure out the precise reasons due to the fact that the component temperatures are not available in the all pixels because the inversion technique is limited by the surface conditions and the directional signature captured by the satellite. A more detailed study needs to be done to investigate the reasons.
- The results from RACMO model show the trend of larger values either than observations or the estimations by SEBS in most cases. The RMSD between SEBS and RACMO model estimations is as large as up to about 75 W m^{-2} (Fig.6). More detailed investigation are needed to find out the reasons. The present work may prove significant for the validation of mesoscale atmospheric models. We notice that previous validations are usually done for near surface temperature and humidity, only indirectly related to heat fluxes. We believe that this study is the first case that has used a scaling techniques to evaluate the fluxes of a mesoscale at a grid scale.
- There are apparent discrepancies between the roughness for momentum transfer used in SEBS and in RACMO. The consequences of such difference needs to be investigated.

On the basis of this experimental validation, it is concluded that SEBS can be used to estimate turbulent heat fluxes at different scales with acceptable accuracy. Finally, the application of SEBS does not require any a priori knowledge of the actual turbulent heat fluxes, indicating that SEBS is a credible and independent approach. Due to this property, SEBS results may be used for validation and initialisation of hydrological, atmospheric and ecological models that usually require proper partition of the sensible and latent heat flux at different scales. SEBS results may also be used via data assimilation in the above models to increase the reliability of the model simulations and predictions.

WP 7: Assimilation of surface fluxes and moisture indicators into NWP

In Workpackage 7 a range of activities have taken place. This section first gives a brief overview of data assimilation procedures and experiments that have been carried out in earlier BCRS-funded projects (both in the NRSP and GO programmes). Then, progress in the development of more advanced and efficient data assimilation procedures and cost functions is reported. As a final contribution to this workpackage, the land surface parameterisation scheme in the KNMI model RACMO was extended with a semi-empirical sub-model for the roughness ratio z_{om}/z_{oh}, as developed by Su et al (2001). The formulation and evaluation of this submodel is reported here.

Overview of recent developments

In the context of a range of projects supported by BCRS and ESA, the present consortium has spent a fair amount of attention to the way advanced land surface observations can be assimilated into an atmospheric limited area model used for Numerical Weather Prediction (NWP). The work started with assimilation of surface evaporative fraction estimates obtained by using the Surface Energy Balance Algorithm for Land (SEBAL) into a NWP, as reported by Van den Hurk et al (1997). Since this early work, further development of NWP data assimilation was carried out along two lines. The first line was built on the consideration that the accuracy of land surface flux estimates could be improved by a combination of a revised surface flux retrieval algorithm (Surface Energy Balance Index, or SEBI) and making use of new observations that would become available from MSG and ENVISAT sensors. This resulted in the work reported in the final report of Phase 1 of this study (Su and Jacobs, 2001) and in Workpackages 5 and 6 of this project. In particular, experiments were carried out in which directional surface temperatures – leading to estimates of canopy and underground temperatures – were assimilated into a tiled land surface scheme in the KNMI model RACMO (Van den Hurk et al, in press).

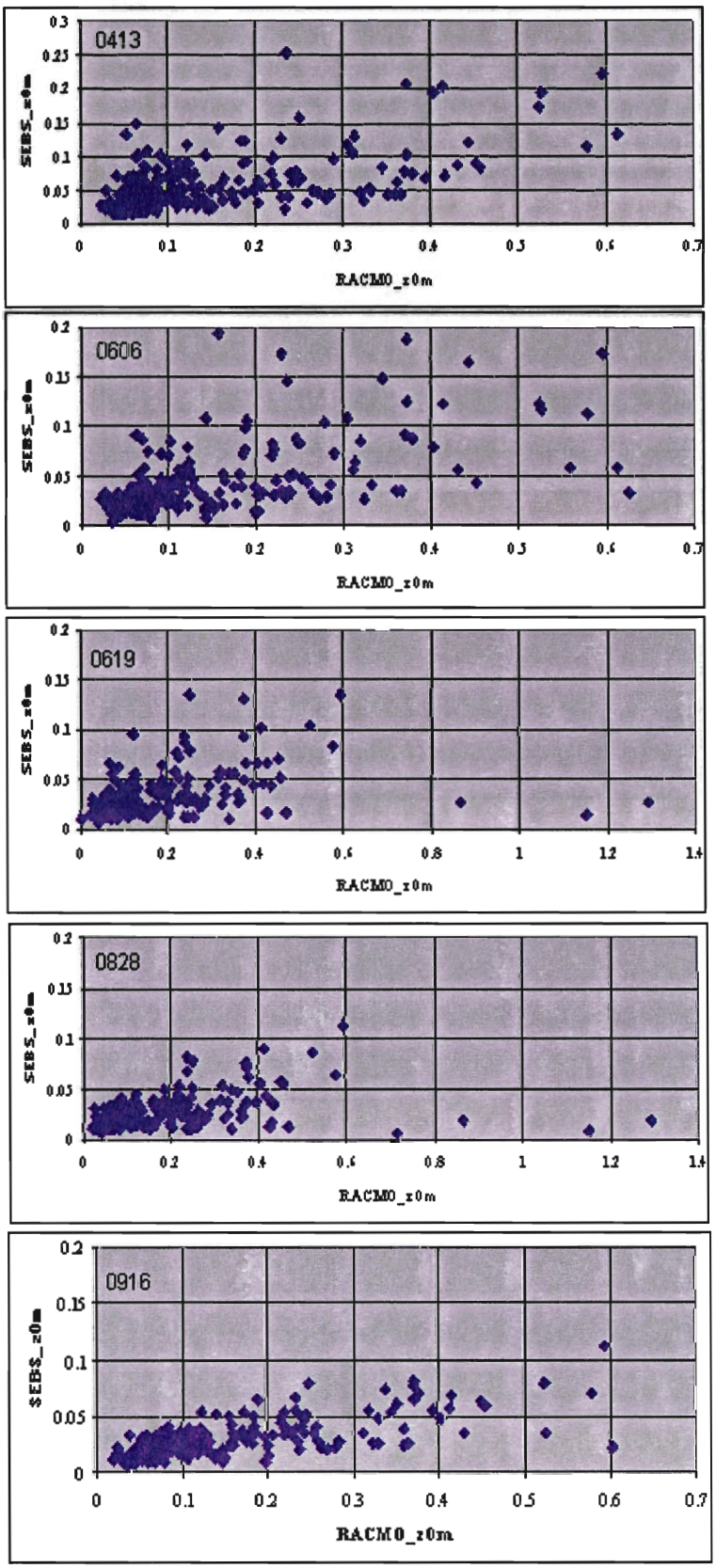

Fig. 6.3 The comparison of z_{0m} between SEBS and RACMO, each panel showing one of 5 days in 1999

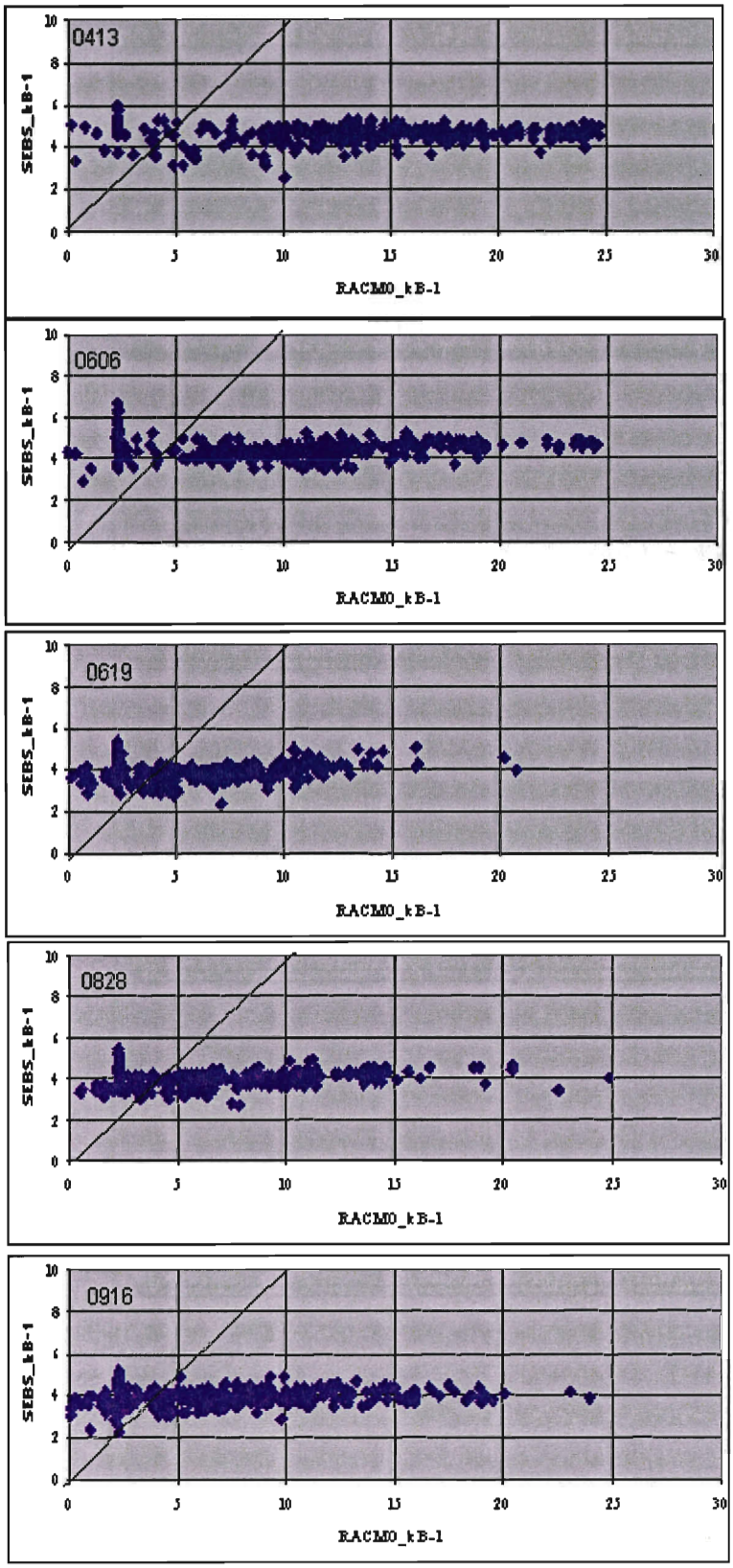

Fig. 6.4 The comparison of kB^{-1} between SEBS estimation and values in RACMO model.

Table 6.4 The comparison of sensible heat flux (W m^{-2}) between measurements by scintillometer and the estimation by SEBS (- denotes there is no estimation due to lack of input variables; * denotes too few pixels available to carry out the standard deviation).

Site and image	Obs. Mean H	Single-source estimation		Dual-source estimation		Statistics over RACMO grid		RACMO H
		mean H	std H	mean H	std H	mean H	Std H	
Tomelloso								
990413	289.6	308.7	5.1	-	-	312.2	14.9	343.4
990606	280.9	272.2	7.3	-	-	243.7	59.9	378.3
990619	209.7	206.8	15.5	-	-	230.5	32.8	386.2
990828	220.9	212.1	6.0	-	-	215.9	11.7	286.9
990916	191.1	163.4	11.8	-	-	169.6	36.3	183.9
Lleida								
990715	187.7	210.5	11.9	-	-	224.6	51.6	223.0
990721	179.5	149.1	23.7	101.7	*	174.2	48.3	194.6
990929	152.8	94.0	33.2	103.4	34.1	119.9	57.4	110.3
Badajoz								
990730	173.3	164.6	26.2	175.7	*	146.0	43.5	213.2
990815	126.4	108.8	17.5	-	-	108.3	21.5	170.9
990821	154.8	129.9	13.1	185.9	*	133.1	34.9	193.2

A second line of data assimilation work was based on the relationship between surface moisture conditions and the rate of surface temperature increase after sunrise, the so-called heating rate. In Phase 1 of this project, a case study is described in which METEOSAT derived heating rates are assimilated into RACMO. This line will be further explored in the context of the EU-funded project ELDAS (European Land Data Assimilation System) coordinated by KNMI. The formulation of ELDAS has been significantly inspired on activities carried out in the context of BCRS-funded projects, including Phase 1 of the current project.

Data assimilation procedures

The two lines of research described above address the value of the various types of geophysical information that may be extracted from routine or advanced land surface observations. Parallel to these developments, attention has been paid to various numerical schemes that are available for assimilation of this information into a NWP environment. The early SEBAL work (Van den Hurk et al, 1997) used a simple direct insertion method, in which soil moisture fields in RACMO were modified in order to match SEBAL derived evaporative fractions directly, without taking notice of possible observation errors or model quality. The early attempts to assimilate directional surface temperatures (Van den Hurk et al, in press) made use of a (complicated) minimisation scheme, that searched the value of a combination of roughness and soil moisture quantities that would optimise a cost function measuring the distance between modelled and observed quantities in a statistical way. This so-called variational minimisation method acknowledges the limited accuracy of observations, and is able to define a balance between the skill of the model and the

skill of the observations. However, the minimisation scheme used so far required a large number of full NWP integrations, and was not always able to find the optimal solution. The work carried out with the METEOSAT heating rates yielded a variational minimisation scheme that was both effective and efficient, and this method was subsequently also applied to the directional temperature assimilation. A brief description of the comparison between the two minimisation schemes is given below.

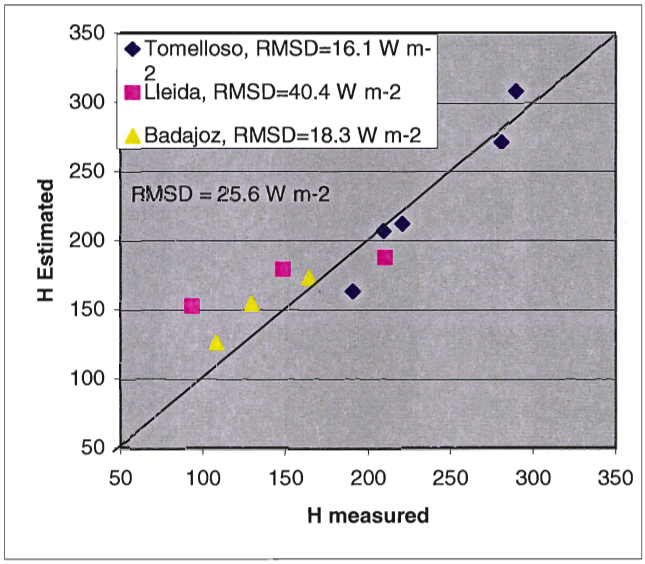

Fig. 6.5 The agreement of H estimated by SEBS with observations. Each symbol represents one time interval in which an ATSR derived surface flux estimation and half hourly averaged surface observations were both available.

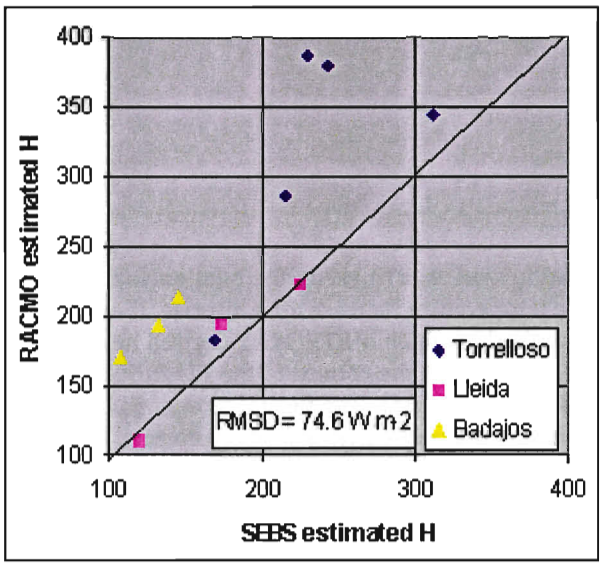

Fig. 6.6 The comparison of H estimated by SEBS and RACMO model.

The first (complex) minimisation method consisted of a combination of a parabolic interpolation and a conjugate gradient determination (Press et al, 1989). The task of the method is to find the minimum of an arbitrarily shaped cost function J, which is defined as

$$J = \sum \left[\frac{x_m - x_o}{\sigma_o} \right]^2 \qquad (7.1)$$

in which x_m is a modelled quantity (say, component surface temperature separately for canopy and underground), x_o the observed equivalent, and σ_o the specified observation error. The modelled surface temperatures vary by changing the soil moisture content and by changing the aerodynamic coupling between the surface and the atmosphere, implemented by changing the roughness ratio z_{om}/z_{oh}. Thus J may be considered as a multidimensional function of soil moisture content w and z_{om}/z_{oh}. The minimum of J is supposed to be at a location where w and z_{om}/z_{oh} take their preferred values.

The minimisation procedure starts with executing a NWP run with a default value of w and z_{om}/z_{oh}. An initial search direction $[\Delta w, \Delta z_{om}/z_{oh}]$ is also specified. In this search direction, J is evaluated at a number of locations assuming a parabolic shape of J. At the location of $[\Delta w, \Delta z_{om}/z_{oh}]$ where the minimum of J is found, a new search direction is defined, and the parabolic minimisation procedure is repeated.

Each evaluation of J requires a full NWP integration, to calculate the effect of changing w and z_{om}/z_{oh} on J. Typically 25 NWP runs are necessary to find a reasonable minimum of the cost function.

This rather expensive procedure was simplified drastically by Hess (2001), who made the following assumptions:

- In a sequential data assimilation experiment, the first guess value of the control variables (w, z_{om}/z_{oh}) is not far away from the optimal values. Search in only one direction should be sufficient to find a reasonable minimum
- Close to the minimum, the gradient of the cost function with respect to the control variables can be estimated by a linear function. This is equivalent to assuming that J is a quadratic function of the control variable x. A new minimum can effectively be found from assessing $\partial J/\partial x$ at the position of the first guess of x.

The combination of these two assumptions enables to make an estimate of the new minimum of J by determining $\partial J/\partial x$ for each control variable x by a finite difference approach, i.e. requiring only one additional run with the NWP model for each x.

In the following example we have examined the assumptions made by Hess (2001) for one of the NWP data assimilation experiments in which directional surface temperatures were used to adjust soil moisture content and roughness ratio in RACMO. We have done so by applying the search procedure of Hess (2001) twice: once from an arbitrary first guess background obtained from a previous (unassimilated) RACMO run, and once again from the optimum fields of w and z_{om}/z_{oh} that resulted from this first optimisation. If the assumptions made are valid, this second iteration should yield results that are close to the results of the first iteration.

Figure 7.1 shows the comparison of ln z_{om}/z_{oh}, found from the first and second iteration of the minimisation procedure in which ATSR derived directional surface temperatures were used to update this roughness ratio in RACMO. It appears that the 1st iteration yielded results that are hardly changed anymore when an additional iteration is carried out, implying that the procedure yields estimates of ln z_{om}/z_{oh} that are close to the optimum that could be found from the comparison of RACMO surface temperatures and ATSR data. This example shows that the simple linear approximation of the cost function minimisation provides an efficient and effective way to perform the data assimilation. Additional experimentation by Hess (2001) confirms this result also for other sources of observations used to adjust soil moisture fields in NWP models. The procedure will further be developed and finetuned in the context of ELDAS, and will be applied in the following data assimilation experiments.

Formulation of the cost function

The cost function as formulated by equation 7.1 measures the difference between observed and modelled quantities, normalised by the noise that occurs due to limited data accuracy. However, it ignores a penalty for violating the physical evolution of the modelled control variables. This is normally taken care of by adding a so-called background term to the cost function, which confines modifications to the first guess values of these control variables by comparing these modifications to a specified background model error. The full equation for J then becomes

$$J = \sum \left[\frac{x_m - x_o}{\sigma_o} \right]^2 + \sum \left[\frac{\Delta w}{\sigma_w} \right]^2 \qquad (7.2)$$

where Δw is the modification to control variable w, and σ_w is the model background error. The results of a data assimilation procedure using a cost function as described by equation 7.2 is governed by the (a priori) choices of the observation and background errors, or the ratio between these. In the experiments described below we have chosen to set the background error at relatively high values, to estimate the maximum effect the satellite observations may have on the NWP forecast.

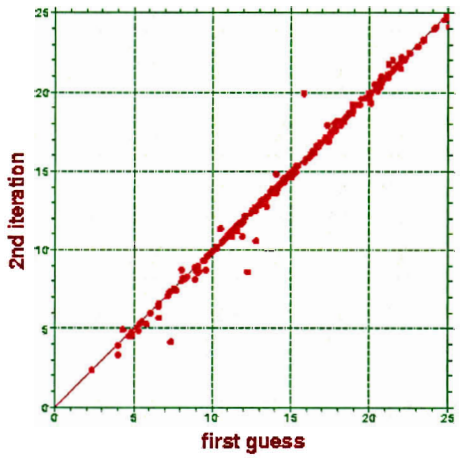

Figure 7.1: example of the effect of the number of iterations on the resulting value of ln z_{om}/z_{oh}, applied to the ATSR image of 13 April 1999. 'First guess' refers to the primary iteration of the minimisation procedure. Each symbol in the figure represents one RACMO grid box for which ATSR data were used to update the roughness ratio value.

An appropriate choice for the observation error is difficult to make. In principle, it depends on many aspects related to the observation accuracy of the spaceborne sensor, the atmospheric correction, the retrieval algorithm and the ancillary data that enter the retrieval. For the ATSR case studies discussed below we have followed a pragmatic solution, by relating σ_o to the standard deviation of all pixel temperatures within a NWP gridbox, σ_T, and the number of pixels passing the quality screening (see Workpackage 5), N/N_{max}:

$$\sigma_o = \frac{\max\left[\sigma_{T,s}, \sigma_{T,v}\right]}{N / N_{\max}} \qquad (7.3)$$

where $\sigma_{T,s}$ and $\sigma_{T,v}$ are the standard deviations of the bare ground and canopy temperatures, respectively (see Van den Hurk et al, in press). This formulation of the observation error will give less weight to gridbox averaged surface temperatures when the variability of the component temperatures derived from the ATSR observations is very large, or when only little satellite observations contribute to the representative value. Although σ_T is not necessarily related to the true observation error, it is a practical indicator for the representativity of the measurements on the scale of a NWP grid box.

An evaluation of roughness ratio's obtained by data-assimilation

In the report of Phase 1 of this project a case study is presented in which ATSR derived component temperatures were used to update the soil moisture content and the roughness ratio in the limited area model RACMO. An extensive description of this experiment is also given by Van den Hurk et al (in press), which manuscript is prepared in the context of Phase 2 of the project.

For 5 days in 1999 ATSR images were used to derive component surface temperatures for the Eastern part of the Iberian peninsula, and for one additional day for the surroundings of the Netherlands. The main conclusion of that study was that for the Iberian peninsula the aerodynamic properties of the surface (the roughness ratio z_{om}/z_{oh}) had to be adjusted to significantly higher values than the default constant parameter in order to match RACMO and ATSR derived surface temperatures.

The section concerning Workpackage 6 gives a detailed description of a semi-empirical model for this roughness ratio, as developed by Su et al (2001). We have implemented a simplified version of this roughness ratio model in the land surface scheme in RACMO. The simplifications were mainly guided by the availability of (calibration) coefficients that are needed to close the parameterisation. The basic formulation of the roughness sub-model reads

$$\ln\frac{z_{0m}}{z_{0h}} = \frac{kC_d}{4C_t\dfrac{u_*}{u(h)}\left(1-\exp(-n/2)\right)} f_c^2 + \frac{k\dfrac{u_*}{u_h}\dfrac{z_{0m}}{h}}{C_t^*} f_c^2 f_s^2 + kB_s^{-1} f_s^2 \quad (7.4)$$

where C_d and C_t are drag coefficients specified by a constant value, $u_*/u(h)$, z_{om}/h and n are turbulent properties depending on the canopy leaf area index, kB^{-1} is a roughness ratio for the bare ground surface (parameterised depending on a specified bare ground momentum roughness length and a turbulent Reynolds number), and f_c and f_s are the areal coverage of plants and bare ground, respectively (see Workpackage 6 or Su et al, 2001, for details). Equation 7.4 is a simplified version of the original model discussed by Su et al. All coefficient values needed to calculate z_{om}/z_{oh} are solely obtained from vegetation information (leaf area index, vegetation coverage) which is used operationally in the tiled land surface scheme in RACMO.

In addition to the ATSR data assimilation experiments reported in Phase 1, an extra set of RACMO simulations was carried out in which equation 7.4 was implemented to parameterise the roughness ratio of the bare ground tile in the RACMO surface scheme (see Phase 1 report). In these simulations no data assimilation was applied. Instead, the soil moisture fields that were obtained from the earlier data assimilation experiments were used to initialise the soil moisture profiles of the RACMO simulations. The roughness ratio was given by Equation 7.4. The runs were carried out for the same model domains and periods as described in Phase 1 and Van den Hurk et al (in press). All runs were initialised at midnight prior to the day for which ATSR data were available, and lasted 12 hours. Hourly averaged surface sensible heat fluxes and component surface temperatures calculated for the gridboxes in which ATSR data were available were stored.

Figure 7.2 shows a representative example of the effect of the inclusion of equation 7.4 on the surface sensible heat flux (see also next section). The roughness sub-model generates surface sensible heat fluxes which agree closely with the result from the assimilated cases, and are generally lower than the first guess simulations (note the negative sign for upward fluxes). Similar results were obtained for the case studies for the other 4 days in 1999.

Note that in the comparison shown in figure 7.2 the largest difference between the assimilated and first guess runs may come from adjustments of soil moisture content rather than from adjustments in the aerodynamic properties. A comparison of these runs to the RACMO run including equation 7.4 may therefore not reflect only the effect of the kB-model. However, the close correspondence between the assimilated run and the roughness submodel shows that both procedures behave fairly similar. Whether the roughness submodel is a good candidate to replace the data assimilation procedure needs to be explored further in Phase 3.

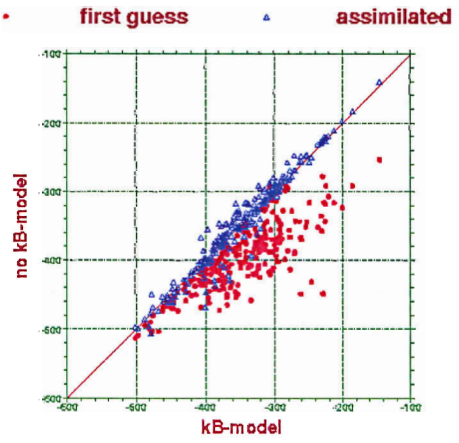

Figure 7.2: Scatterplot of hourly averaged surface sensible heat flux between 10:00 and 11:00 UTC at 19 June 1999 of a RACMO simulation over the Iberian peninsula using equation 7.4 for the roughness ratio on the x-axis, and the same surface flux for the first guess run (red circles) and assimilated run (blue triangles) on the y-axis. Heat fluxes are defined positive downward.

WP 8: Validation of the improvements of the NWP predictions

Bart van den Hurk

The assimilation of satellite derived land surface properties into an NWP system should serve the quality of the forecasts of such a system. When the satellite derived products are physically realistic and compatible with the physical assumptions made in the land surface parameterisation of the NWP model, the data assimilation will bring the model closer to a realistic state. In principle this should be evaluated with comparison of the NWP results to data that are not included in the assimilation. This evaluation should preferably be carried out at the proper spatial scale, that is, at the scale at which the NWP data operates. For the examples discussed earlier, beneficial effects are to be expected for the general surface flux partition in the whole Iberian peninsula, or at least in those parts where satellite data were available and could be assimilated in the model.

Routine surface flux measurements are not available at this scale. As an alternative, forecast scores of near-surface quantities (relative/specific humidity, temperature) have been examined in the past (e.g. Van den Hurk et al, 1997), as a proxy to the surface turbulent fluxes. This evaluation was carried out also with the limited assimilation experiments reported in Phase 1 of the project and by Van den Hurk et al (in press). Assimilation of ATSR-2 component temperatures appeared to be slightly beneficial to the 2m temperature, but relative humidity results were not improved.

At a later stage in Phase 3, it is foreseen that SEBI surface fluxes will be assimilated into the RACMO model, but this is not yet carried out. As an intermediate evaluation, we have briefly analysed the surface flux predictions for the Tomelloso location for various runs of the RACMO model. This analysis was also presented in Workpackage 6, discussed above (Table 6.4).

Three RACMO runs were available for each of the 5 days in 1999 for which for that location component temperatures were obtained: the first guess simulation (shown in Table 6.4), the simulation in which ATSR-component temperatures were assimilated by changing the soil moisture content and the roughness ratio, and one simulation in which the assimilated roughness ratio is replaced by the kB-model by Su et al (see Workpackage 7).

Figure 7.1 shows the correspondence between the ground-truth observations carried out with the scintillometer device in the Tomelloso area with the various RACMO runs. For reference, also the single source model estimate discussed in Workpackage 7 is displayed.

It is clearly seen that the assimilation of surface temperatures gives lower sensible heat fluxes, and in general improves the correspondence with the observations. However, the fluxes are still relatively high compared to the single source model and the ground observations. The degrees of freedom in the data assimilation are apparently too small to produce a model state that is close to the observation. In other words, remaining overestimation of surface sensible heat flux may be the result of too high net radiation in RACMO, too small adjustments in the roughness ratio or soil moisture content, or errors in the parameterisation of the dependence of surface fluxes on various quantities.

The replacement of the assimilated roughness ratio by the simplified kB-model, as discussed in the previous workpackage, does not result in large differences, as was already noted. This implies that incorporating the kB-model does not deteriorate the results that can be expected from the data assimilation exercise, which is good news. On the other hand, it may well be possible that the roughness ratio is not a very important parameter in determining the surface heat flux. In general, the calculated surface heat flux in an interactive land surface scheme is bound severely by available energy, and surface temperatures are dependent quantities rather than quantities that govern the amount of heat transfer. In contrast, satellite flux retrievals are extremely sensitive to the roughness formulation since the (observed) surface temperature is directly used to calculate the heat flux and may not be regarded as a dependent variable. A proper evaluation of kB-models should therefore be carried out by inspection of surface temperatures rather than by looking at surface heat fluxes alone. This requires a well-designed data assimilation experiment in which the kB-model is enabled to play an active role. Such an experiment will be conducted in Phase 3 of the project.

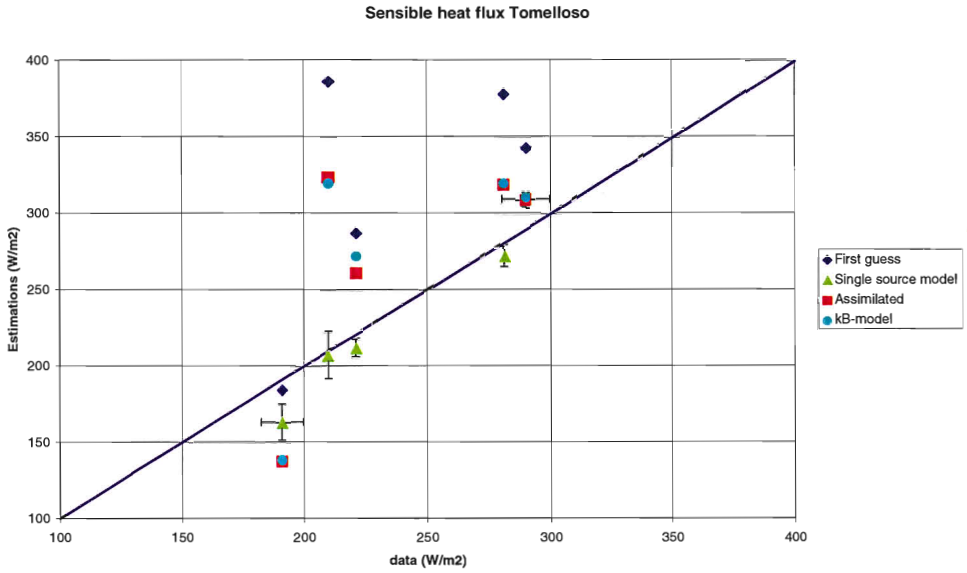

Figure 7.1: Scatter plot of observed sensible heat flux at the Tomelloso site versus various model values of this flux for 5 days in 1999. Shown are model calculations with RACMO without data assimilation ("first guess", als shown in Table 6.4), the single source model discussed in Workpackage 6, the assimilated RACMO run, and a RACMO run with the kB-model by Su et al (2001).

Executive Summary

Results achieved

During the 2nd phase of the current ENVISAT- Land Surface Processes project, a number of activities have been carried out that further pave the way towards the use of ENVISAT land surface data in a NWP environment.

Referring to the retrieval of albedo, leaf area index and atmospheric corrections, preliminary radiative transfer calculations have been carried out that should enable the retrieval of these parameters once AATSR and MERIS data become available. However, much of this work is still to be carried out. An essential part of work in this area is the design and implementation of software that enables an efficient use of MODTRAN4 radiative transfer code, and during the current project phase familiarization with these new components has been achieved.

Surface emissivity, a small workpackage, has not received any attention. It is foreseen that this workpackage will no longer be included in the next phase of the report, since reasonable results are not anticipated from the limited resources made available for this part of the work.

Significant progress has been made with the retrieval of component temperatures from directional ATSR-images, and the calculation of surface turbulent heat fluxes from these data. The impact of vegetation cover on the retrieved component temperatures appears manageable, and preliminary comparison of foliage temperature to air temperatures were encouraging. The calculation of surface fluxes using the SEBI concept,which includes a detailed model of the surface roughness ratio, appeared to give results that were in reasonable agreement with local measurements with scintillometer devices. The specification of the atmospheric boundary conditions appears a crucial component, and the use of first guess estimates from the RACMO models partially explains the success.

Earlier data assimilation experiments with directional surface temperatures have been analysed a bit further and were also compared to results obtained from directly modelling the surface roughness ratio. Results between these calculations and the data assimilation results appeared well comparable, but a full test in which the surface roughness model is allowed to play a free role during the data assimilation process has yet to be carried out.

Tasks in Phase 3

Although some progress was reported during the current phase, a number of tasks has still to be carried out before the project can be considered to be succesfully completed. This is due to a combination of a lack of availability of ENVISAT data, and the limited extent (9 months) of the current 2nd phase.

On the retrieval side, sample products of leaf area index and albedo still have to be generated, and their quality has to be assessed in an NWP environment. The same holds for the atmospheric correction from MERIS data.

Surface component temperature retrieval algorithms have matured more and more, but reliable validation, for instance using very high resolution imagery in which vegetation and bare ground pixels can be separated, has yet to be carried out. The calculation of surface fluxes has to be completed towards the regional scale, which enables the assimilation of these fluxes into an NWP. Spatial and temporal variability of these fluxes have yet to be analysed.

Data assimilation experiments have yet to develop towards the assimilation of retreived surface fluxes rather than the component temperatures, and temporal and spatial dynamics of these input data has to be analysed. Also verification of the assimilated products using forecast scores of near-surface quantities has yet to be carried out.

We will submit a continuation proposal covering the 3rd phase of the "ENVISAT – Land surface process" project to the GO-call that is anticipated to appear in 2002.

Scientific Publications in the context of the project

Jia, L., Z.-L. Li, M. Menenti, Z. Su, W. Verhoef and Z. Wan (submitted): A practical algorithm to infer soil and foliage component temperatures from bi-angular ATSR-2 data, *International Journal of Remote Sensing.*

Su, Z., T. Schmugge, W.P. Kustas, W.J. Massman, An evaluation of two models for estimation of the roughness height for heat transfer between the land surface and the atmosphere. J. Appl. Meteorology, 40(11), 1933-1991, 2001.

Van den Hurk, B.J.J.M., Jia, L., Jacobs, C., Menenti, M., and Li, Z.-L., (in press), Assimilation of land surface temperature data from ATSR in an NWP environment – a case study, accepted by *International Journal of Remote Sensing.*

Van den Hurk, B.J.J.M. and H. The (submitted): Assimilation of satellite derived surface heating rates in a Numerical Weather Prediction model; Submitted to Advances of Water Resources

References

Asrar, G., Myneni, R.B. and Choudhury, B.J., Spatial heterogeneity in vegetation canopies and remote sensing of absorbed photosynthetically active radiation: a modeling study, Remote Sensing Environ., 41, 85-103, 1992.

Bach, H., W. Verhoef and K. Schneider, 2000, "Coupling remote sensing observation models and a growth model for improved retrieval of (geo)biophysical information from optical remote sensing data", *Remote Sensing for Agriculture, Ecosystems and Hydrology*, SPIE Vol. 4171, pp. 1-11.

Baret, F., Clevers, J. P. W., and Stevens, M. D., 1995, The robustness of canopy gap fraction estimates from the red and near infrared reflectance. A comparison between approaches for sugar beet canopies. *Remote Sensing Environ.*, 54, 141-151.

Bastiaanssen, W.G.M., Regionalization of surface flux densities and moisture indicators in composite terrain, Ph.D thesis, Wageningen Agriculture University, 1995.

Beck, A., Anderson, G.P., Acharya, P.K. et al., 1999, MODTRAN4 User's Manual. *Air Force Research Laboratory, Hanscom AFB, MA.*

Becker, F., Li, Z.-L., 1995, Surface temperature and emissivity at various scales: definition, measurement and related problems. *Remote Sensing Reviews*, 12, 225-253.

Ehrler, W.L., 1973, Cotton leaf temperatures as related to soil water depletion and meteorological factors. *Agron. Journal*, 65, 404-409.

Brutsaert, W., 1999: Aspects of bulk atmospheric boundary layer similarity under free-convective conditions. *Rev. Geophy.*, 37, 439-451.

Brutsaert, W., and M. Sugita,1992, Regional surface fluxes from satellite-derived surface temperatures(AVHRR) and radiosonde profiles, *Boundary-Layer Meteorology*, 58:355-366.

Finnigan,J.J., M.R.Raupach, E.F,Bradley, and G.K.Aldis,1990, A Wind Tunnel Study of Turbulent Flow over a Two-dimensional Ridge, *Boundary Layer Meteorol.*, 50,277-317.

Flowerdew, R.J. and Haigh, J.D., 1997, Retrieving land surface reflectances using the ATSR-2: A theoretical study. *J. Geophys. Res.*, 102(D14), 17163-17171.

Gausman, H.W., Escobar, D.E., Everitt, J.H., Richardson A.J. and Rodriquez, R.R., 1978, The leaf mesophylls of twenty crops, their light spectra, and geometrical parameters. SWC Research Report 423, Rio Grande Soil and Water Research Center, Weslaco, Texas, 88pp.

Hapke, B., 1981, Bidirectional reflectabce spectroscopy. 1. Theory. *J. Geophys. Res.*, 86, 3039-3054.

Hatfield, J.L., Large scale evepotranspiration from remotely sensed surface temperature, Proc. on planning, now for irrigation and drainage IR Div?ASCE, Lincoln, NE, July 18-21, 502-509, 1988.

Hess, R. (2001): Assimilation of screen-level observations by variational soil moisture analysis; Meteorol.Atm.Phys. 77, 145-154.

Jackson, R.D., 1982, Canopy temperature and crop water stress, *Advances in Irrigation*, 1, 43-85.

Jia, L., Z.-L. Li, Z. Su, C. Jacobs, M.P. Stoll, M. Menenti, "Synergistic use of ATSR-2 multispectral and dual-angle data for land surface studies, *ERS-ENVISAT Symposium: Looking down to Earth in the New Millennium*, 16-20 October, Gothenburg, Sweden, ESA SP-461, CD-ROM, 7pages, 2000.

Jia, L., Z.-L. Li, M. Menenti, Z. Su, W. Verhoef and Z. Wan, A practical algorithm to infer soil and foliage component temperatures from bi-angular ATSR-2 data, *International Journal of Remote Sensing*, (in review), 2001.

Jia, L., Menenti, M., Su, Z.B., Djepa, V., Li, Z.-L. and Wang, J., 2001, Modeling sensible heat flux using estimates of soil and foliage temperatures: the HEIFE and IMGRASS experiments. In "Remote sensing and climate modeling: Synergies and Limitations" in "Advances in Global Change Research", edited by M. Beniston and M. Verstraete (Dordrecht: Kluwer).

Kimes, D. S., 1980, Effects of vegetation canopy structure on remotely sensed canopy temperatures. *Remote Sensing Environ.*, 10, 165-174.

Kimes, D. S., 1983, Remote sensing of row crop structure and component temperatures using directional radiometric temperatures and inversion techniques. *Remote Sensing Environ.*, 13, 33-55.

Kimes, D. S., and Kirchner, J. A., 1983, Directional radiometric measurements of row-crop temperatures. *Int. J. Remote Sensing*, 4, 299-311.

Klesspies, T.J. and McMillin, L.M., 1990, Retrieval of precipitable water from observations in the split-window over varying surface temperature. *J. Appl. Meteorol.*, 29, 851-862.

Lagouarde, J. P., Kerr, Y., and Brunet, Y., 1995, An experimental study of angular effects on surface temperature for various plant canopies and bare soils. *Agric. and For. Meteorol.*, 77, 167-190.

Li, Z.-L., Stoll, M.P., Zhang, R.H., Jia, L., and Su, Z., 2001a, On the separate retrieval of soil and vegetation temperatures from ATSR2 data. *Science in China, series D*, 44, 97-111.

Li, Z.-L., M.P. Stoll, R.H. Zhang, L. Jia and Z. Su, Study on the estimation of soil and vegetation component temperatures from ATSR2 data, *Science in China*. E30: 27-38, 2000.

Li, Z.-L., Jia, L., Su, Z., Wan, Z.M., and Zhang, R.H., 2001b, Towards an Operational Algorithm for Retrieving Atmospheric Water Vapor Content From ATSR2 Split-Window Channel Data. Submitted to *J. geophys. Res.*(in review).

Mackay, G. and Steven, M.D., 1998, An atmospheric correction procedure for the ATSR-2 visible and near infrared land surface data. *Int. J. remote Sensing*, 19(15), 2949-2968.

Massman, W.J., 1997: An analytical one-dimensional model of momentum transfer by vegetation of arbitrary structure. *Boundary-Layer Meteorol.*, 83, 407-421.

Massman, W.J., 1999: A model study of kB_H^{-1} for vegetated surfaces using 'localized near-field' Lagrangian theory. *J. Hydrol.*, 223, 27-43.

Massman, W.J., (1999b) Molecular diffusivities of Hg vapor in air, O_2 And N_2 near STP and the kinematic viscosity and the thermal diffusivity of air near STP, *Atmos. Environ.*, 33, 453-457.

Menenti, M., L. Jia, Li, Z.-L., Djepa, V., Wang, J., Stoll, M.P., Su, Z.B. and Rast, M., 2001, Estimation of soil and vegetation temperatures with multi-angular thermal infrared observations: IMGRASS, HEFEI, SGP 1997 experiments. *J. geophys. Res.*, 106, 11997-12010.

Menenti, M. and B.J. Choudhury, 1993. Parameterization of land surface evapotranspiration using a location-dependent potential evapotranspiration and surface temperature range. In: H.J. Bolle et al. (eds.). *Exchange processes at the land surface for a range of space and time scales.* IAHS Publ. No. 212: 561-568

Miller, E.C., and Saunders, A.R., 1923, Some observations on the temperature of the leaves of crop plants, *J. Agric. Res.*, 26, 15-43.

Nielsen, D.S., Clawson, K.L., and Blad, B.L., 1984, Effect of solar azimuth and infrared thermometer view direction on measured soybean canopy temperature. *Agron. J.*, 76, 607-610.

Norman, J.M., Kustas, W.P., and Humes, K.S., 1995, A two source approach for estimating soil and vegetation energy fluxes from observations of directional radiometric surface temperature. *Agric. and Forest Meteorol.*, 77, 263-293.

North, P.R.J., Briggs, S.A., Plummer, S.E. and Settle, J.J., 1999, Retrieval of land surface bi-directional reflectance and aerosol opacity from ATSR-2 multiangle imagery. *IEEE transactions on Geoscience and Remote Sensing*, 37(1), 526-537.

Press, W.H., Flannery, B.P., Teukolsky, S.A. and Vetterling, W.T., 1989, *Numerical recipes*, Cambridge, U.K., Cambridge Univ. Press.

Prévot, L., Brunet, Y., Paw U, K.T., and Seguin, B., 1994, Canopy modelling for estimating sensible heat flux from thermal infrared measurements. *Proc. Workshop on Thermal Remote Sensing of The Energy And Water Balance Over Vegetation in Conjunction With Other Sensors* (La Londe), 17-22.

Rahman, H. and Dedieu, G., 1994, SMAC: a simplified method for the atmospheric correction of satellite measurements in the solar spectrum. *Int. J. remote Sensing*, 15, 123-143.

Raupach, M.R., Drag and Drag partition on rough surfaces, Boundary-Layer Meterology, 60: 375-395, 1992.

Saunders, R.W. and Kriebel, K.T, 1988, An improved method for detecting clear sky and cloudy radiances from AVHRR data. *Int. J. remote Sensing*, 9, 123-150.

Smith, J.A., Chauchan, N.S., and Ballard, J., 1996, Remote sensing of land surface temperature: the directional viewing effect, *I.E.E.E Trans Geosci. Remote Sens.*, 13(4): 2146-2148.

Sobrino, J.A., and Caselles, V., 1990, Thermal Infrared radiance model for interpreting the directional radiometric temperature of a vegetative surface. *Remote Sensing Environ.*, 33, 193-199.

Sobrino, J., Li. Z.-L., Stoll, M.P. and Becker, F., 1994, Improvements in the split-window technique for land surface temperature determination. . *IEEE transactions on Geoscience and Remote Sensin.*, 32(2), 243-253.

Su Z. and C., Jacobs (Editors), *Advanced Earth Observation - Land Surface Climate"*, Publications of the National Remote Sensing Board (BCRS), USP-2, 01-02, 184pp, 2001.

Su, Z., A Surface Energy Balance System (SEBS) for estimation of turbulent heat fluxes from point to continental scale, in Su Z, Jacobs J, (eds.), Advanced Earth Observation – Land Surface Climate, Publications of the National Remote Sensing Board (BCRS), USP-2, 01-02: 91-108, 2001.

Su, Z., T. Schmugge, W.P. Kustas, W.J. Massman, An evaluation of two models for estimation of the roughness height for heat transfer between the land surface and the atmosphere. J. Appl. Meteorology, 40(11), 1933-1991, 2001.

Van den Hurk, B.J.J.M., W. Bastiaanssen, H. Pelgrum and E. van Meijgaard (1997): A new methodology for initialization of soil moisture fields in numerical weather prediction models using METEOSAT and NOAA data; J. Applied Meteorology 36, 1271-1283.

Van den Hurk, B.J.J.M., Jia, L., Jacobs, C., Menenti, M., and Li, Z.-L., (in press), Assimilation of land surface temperature data from ATSR in an NWP environment – a case study, accepted by *International Journal of Remote Sensing.*

Verhoef, W, 2001, Development of algorithms for estimation of atmospheric and surface physical parameters. In: Final Report of Advanced Earth Observation – land surface climate, Report USP-2, Alterra Green World Research, Wageningen UR, the Netherlands, Edited by Su, Z. and Jacobs, C., 2001.

Verhoef, W. and M. Menenti (eds.), 1998, "Final report Spatial and Spectral Scales of Spaceborne Imaging Spectro-radiometers (SASSSIS) ", NLR-CR-98213, NLR, Amsterdam, 289 pp.

Verhoef, W., 1998, "Theory of radiative transfer models applied in optical remote sensing of vegetation canopies", PhD thesis, Wageningen Agricultural University, 310 pp.

Vermote, E.F., Tanre, D., Deuze, J.L., Herman, M. and Morcrette, J.-J., 1997, Second simulation of the satellite signal in the solar spectrum, 6S: An overview. *IEEE transactions on Geoscience and Remote Sensing*, 35, 675-686.

Annexes

Report of the kick-off meeting (in Dutch)

KNMI, 19 april 2001
Aanwezig: Massimo Menenti, Bob Su, Wout Verhoef en Bart vd Hurk (voorz/not)

Hieronder volgt een weergave van de plannen en afspraken die er per werkpakket in het ENVISAT 2001 voorstel zijn opgesteld. De nadruk ligt op de deliverables die er aan het eind van het lopende kalenderjaar (2001) worden verwacht. Verder wordt aangegeven wat de verwachte activiteiten in 2002 zullen zijn indien het vervolgvoorstel wordt goedgekeurd.

Vooraf een aantal losse opmerkingen:

- Massimo heeft via een projektaanvraag bij ESA goedkeuring gekregen voor het bestellen van maximaal 40 ATSR opnames ten behoeve van o.a. dit GO-2 projekt. Aanvragen daarvoor moeten via Massimo bij ESA worden ingediend.
- Het aanverwante SRON project waarin Li Jia's promotie zal worden voltooid heeft goede reviews gehad, en we gaan ervan uit dat dit project zal worden gehonoreerd. Dit betekent dat zij haar werkzaamheden zoveel mogelijk op haar promotie zal moeten richten, en niet teveel belast moet worden met korte klussen die in het kader van o.a. dit GO-2 project moeten worden uitgevoerd.
- Wout is er niet helemaal zeker van of hij de geplande uren voor 2001 daadwerkelijk aan het projekt zal kunnen besteden. Zodra evt. blijkt dat er een verschuiving naar 2002 nodig is zal Bart ism BCRS een oplossing zoeken.
- Zodra KNMI een contract heeft ontvangen zal Bart voor een opdrachtbrief aan Alterra en NLR zorgen.
- Per kwartaal worden voortgangsrapportages verwacht. Bart zal hiervoor het nodige materiaal verzamelen.
- Op maandag 24 september, 10:00, zal er een voortgangsvergadering plaatsvinden op NLR.

Werkpakket 1: albedo
Er zijn twee kernactiviteiten gepland:

- Het verder onderzoeken van de reden waarom een albedo-berekening met OSCAR voor de ATSR spectrale configuratie slecht valideert met ATSR data.
- Het onderzoeken van de mogelijkheden om met de programmeerbare MERIS sensor nauwkeurige albedo metingen te doen. Dit wordt onderzocht met hyperspectrale metingen van de HYMAP sensor. Wout neemt contact op met Massimo en Jose Moreno voor de HYMAP data.

Werkpakket 2: Leaf area index
Het doel is het ontwikkelen van een bruikbaar algoritme om LAI schattingen te doen op basis van AATSR & MERIS metingen. De activiteiten bestaan uit:

- Onderzoeken van de meerwaarde van de bidirectionele (A)ATSR data voor de schatting van LAI dmv numerieke simulaties
- Validatie van LAI metingen voor het Barrax gebied aan de hand van hyperspectrale HYMAP metingen (zie WP 1).
- Alterra zal een validatie uitvoeren voor de Chinese IASIS campagne, waarvoor grond- en ATSR-waarnemingen beschikbaar zijn.

Gedurende 2001 zal er uitsluitend met ATSR metingen voor Nederland en Spanje (1998/1999) en China (2001) worden gewerkt, in 2002 (indien mogelijk) ook met ENVISAT data.

Werkpakket 3: Atmosferische parameters

Het doel van dit werkpakket is het ontwikkelen en testen van methoden om atmosferische parameters te bepalen op basis van MERIS metingen boven land. Dit zal worden gedaan door mbv MODTRAN4 simulaties en de regressie met waterdamp en aerosol optische dikte te vertalen naar systeemparameters die voor de MERIS spectrale banden de stralingsinteracties beschrijven in het ensemble atmosfeer-aarde. Een test zal worden uitgevoerd met (opnieuw) de HYMAP waarnemingen van Jose Moreno, waarvoor zowel een set ruwe data (op 4km hoogte) als atmosferisch gecorrigeerde grondwaarnemingen aanwezig is. De vereenvoudigde atmosferische correctie zal hiermee worden vergeleken.

In 2001 zal met name de infrastruktuur worden opgezet en de MODTRAN4 simulaties worden gegenereerd, en in 2002 zal de test worden uitgevoerd.

Alterra zal zich gaan toeleggen op praktische algoritmes voor de correctie van de thermische AATSR waarnemingen.

Werkpakket 4: Emissivity

Dit is een erg klein werkpakket. Het oorspronkelijke plan om emissivity-modellen te maken voor ATSR 11&12μ kanalen is theoretisch nauwelijks uitvoerbaar. Bob Su zal proberen om een set ASTER dataset te bemachtigen waarmee een eenvoudige emissiviteits-relatie (bv als functie van vegetatie indices) kan worden getest.

Werkpakket 5: Directionele temperatuurretrieval en validatie

Dit werk staat in relatie tot het promotiewerk van Li Jia. Kernactiviteit is het valideren van component oppervlaktetemperaturen uit ATSR voor de IASIS en DAISEX campagnes. De bijdrage voor participatie in veldcampagnes is gerechtvaardigd door Bob's bemoeienissen met de plaatsing van scintillometers voor de IASIS campagne. Verder heeft Jiemin Wang gevraagd om een periode op Alterra te komen werken. Indien zijn werkzaamheden passen in het kader van dit projekt (bv. validatie van opp.temperaturen of fluxen) kan ook dit worden gefinancierd uit het campagnegeld van Alterra.

Werkpakket 6: Sensible and latent heat fluxes

Voor 2001 is het noodzakelijk dat er flux-schattingen worden gemaakt aan de hand van de ATSR beelden van Cabauw en Spanje (1998/1999) en worden gevalideerd met scintillometer-data (Spanje 1999) of fluxschattingen mbv operationele synops waarnemingen. Bart zal deze fluxschattingen aan Bob sturen. De fluxen zullen worden gegenereerd met zowel het single component SEBS algoritme als met een dual source model. Bob zal inhoudelijk aan deze fluxschattingen werken, en evt. assistentie krijgen van studenten t.a.v. de validatie (Katja Sintonen en Han Rowerda). Li Jia kan evt. de begeleiding van de studenten verzorgen, maar moet zoveel mogelijk worden ontzien met het oog op haar promotie.

Voor 2002 zullen verdere validaties met andere campagnes op de agenda worden gezet.

Werkpakket 7: Variationele assimilatie van fluxen en/of temperaturen

Het werk wat vorig jaar voor ESA/ECMWF is uitgevoerd zal worden verfijnd en uitgebreid met assimilatie van de 1999 ATSR data voor Spanje. Hierbij worden twee onderwerpen behandeld:

- Directe assimilatie van component temperaturen in RACMO door ad hoc aanpassing kB^{-1}
- Simulaties van kB^{-1} dmv Bob's model, en evaluatie van de resulterende oppervlaktetemperaturen

In 2001 zullen de aangepaste kB^{-1} waarden worden vergeleken met Bob's model. Indien er enig succes wordt geboekt bij deze vergelijking zal in 2002 een RACMO simulatie voor heel Europa voor een groot deel van het seizoen worden uitgevoerd met deze kB^{-1} parameterisatie.

Werkpakket 8: Validatie van RACMO fluxen

De resultaten van de runs uit het vorige werkpakket zullen waar mogelijk worden vergeleken met beschikbare fluxdata (scintillometer Spanje, evt andere campagnes waarvoor nieuwe assimilatie runs worden gedraaid).

Report of progress meeting

NLR, 27 September 2001

Attending: Wout Verhoef, Massimo Menenti, Bart van den Hurk (chair/minutes), Li Jia, Gerbert Roerink, Katja Sintonen, Bob Su, Han Rowerda

Agenda

- Progress reports per workpackage
- Continuation in phase 3 (2002)
- Other issues

Progress report per workpackage

WP 1 & 2

Wout Verhoef has found a way to "interrogate" the complex MODTRAN4 atmospheric radiative transfer model in order to extract from its outputs six effective parameters for describing the interaction with the earth's surface. For a given geometry and atmospheric state, this allows one to "forget" MODTRAN4 and apply the six parameters instead, which can easily be done pixel by pixel and at high spectral resolution. The six parameters will now be combined with surface reflectance outputs obtained from the combination PROSPECT/SAIL in order to model the dependence of TOA radiances on vegetation parameters. The new simulation set-up will be used to simulate the observation scenario's of albedo and LAI from AATSR and MERIS. These simulations have not yet been carried out, but this will be done before the end of the year. For WP2 (LAI retrieval) also simulations will possibly be carried out for the airborne sensor flown in IASIS, at least, when the angular sampling of this sensor appears adequate to be simulated. Li Jia will contact the IASIS study team to find out details on the angular sampling, and communicate these to Wout.

WP 3

Wout has prepared a nice and user-friendly tool to help prepare input control files for running MODTRAN4. The tool is publicly available for free at http://remotesensing.nlr.nl. Bart pointed him at the existence of the BCRS ACCE project, which focused on atmospheric corrections from synergistic ENVISAT sensors. Wout will study the ACCE report and contact the study team to explore the possibilities of continuing their work.

WP 4

No progress has been reported

WP 5

Li Jia gave a presentation on modeling work on directional temperature sampling over canopies with varying densities. The analysis of DAISEX data (Barrax 1999), as proposed in the kick-off meeting, has not yet been carried out. A straightforward analysis would be to retrieve canopy and soil temperatures directly from the high resolution DAISEX image, by sampling representative bare/vegetated pixels. This will be carried out during 2001.

WP 6

Han Rowerda analysed flux estimates from SEBI and SEBS using ATSR images for a forest site in the Flevopolder and 4 sites spread over Spain. The flux estimates were compared to scintillometer and eddy correlation data. The skill appeared to be very sensitive to aerodynamic effects (flux-profile relationships, roughness formulations) and probably also to the lack of representativity of atmospheric profiles. Li Jia presented results of a case study where RACMO atmospheric profiles were used, and her analysis of 5 days in 1998 yielded rather good results.

WP 7 & 8

No progress made. Bob Su will present a note on how the (aerodynamic) calibration problems with SEBS/SEBI should be anticipated in the data assimilation and verification experiments yet to be carried out in RACMO. This will be prepared before 20 October.

Continuation in 2002

Massimo presented information that there is a fair chance that the next phase of the GO programme will be approved as proposed by the earlier user consultation meetings. However, since the budget will not

be approved in the Parliament before end December this year, the subsequent call for proposals and their evaluation will not allow a continuation of the GO programme before mid 2002. Since our 3rd project phase was planned to take place in 2002, this will cause a gap in the financial support of this project. The current participants felt that this was not a major problem for the actual continuation of the project, since no staff commitments were yet made.

Other issues

The project participants are asked to send their invoice and quarterly summary report soon to the project coordinator.

List of Acronyms

(A)ATSR	(Advanced) Along-Track Scanning Radiometer
BCRS	Begeleidings Commissie Remote Sensing
BOA	Bottom of Atmosphere
BRDF	Bi-directional Reflectance Distribution Function
DAASCEES	Data Assimilation and Scaling for the Earth Explorer Core Candidate Mission SPECTRA
ERS	European Remote sensing Satellite
IFOV	Instantaneous Field Of View
KNAW	Koninklijke Nederlandse Academie van Wetenschappen
LAI	Leaf Area Index
LAS	Large Aperture Scintillometer
LIDF	Leaf Inclination Distribution Function
MERIS	Medium Resolution Imaging Spectrometer
NDVI	Normalized Difference Vegetation Index
NWP	Numerical Weather Prediction
RACMO	Regional Atmospheric Climate Model
RMSD	Root Mean Square Difference
SASSSIS	Spatial and Spectral Scales of Spaceborne Imaging Spectro-radiometers
SEBAL	Surface Energy Balance Algorithm for Land
SEBI	Surface Energy Balance Index
SEBS	Surface Energy Balance System
SW	Split Window
SWIR	Short Wave Infra-Red
TIR	Thermal Infrared Irradiance
TOA	Top Of Atmosphere

OVERZICHT VAN RECENT VERSCHENEN KNMI-PUBLICATIES

KNMI-PUBLICATIE MET NUMMER

186-III Rainfall generator for the Rhine Basin: nearest-neighbour resampling of daily circulation indices and conditional generation of weather variables / Jules J. Beersma and T. Adri Buishand

186-IV Rainfall generator for the Rhine Basin: multi-site generation of weather variables for the entire drainage area / Rafal Wójcik, Jules J. Beersma and T. Adri Buishand

186-V Rainfall generator for the Rhine Basin : description of 1000-year simulations / J.J. Beersma

189 Aardbevingen in Noord-Nederland in 1998: met overzichten over de periode 1986-1998 / [Afdeling SO]

190 Seismisch netwerk Noord-Nederland / [afdeling Seismologie]

191 Het KNMI-programma HISKLIM (HIStorisch KLIMaat) / T. Brandsma, F. Koek, H. Wallbrink, G. Können

192 Gang van zaken 1940-48 rond de 20.000 zoekgeraakte scheepsjournalen / Hendrik Wallbrink en Frits Koek

193 Science requirements document for OMI-EOS / contr. by R. van der A .. [et al.] **(limited distribution)**

194-1 De zonsverduistering van 11 augustus 1999, deel 1: de waarnemingen van het gedrag van flora en fauna / J. Kuiper, m.m.v. Guus Kauffeld

195 An optimal infrasound array at Apatity (Russian Federation) / Läslo Evers and Hein Haak **(limited distribution)**

196-I Rainfall Generator for the Meuse Basin: simulation of 6-hourly rainfall and temperature for the Ourthe catchment / Rafal Wójcik and T. Adri Buishand

197 Meteorologie op zee: beknopte handleiding voor waarnemingen op zee [= manual meteorology at sea] **(limited distribution)**

TECHNISCH RAPPORT = TECHNICAL REPORT (TR)

228 Evaluation of modified soil parameterization in the ECMWF landsurface scheme / R.J.M. IJpelaar

229 Evaluation of humidity and temperature measurements of Vaisala's HMP243 plus PT100 with two reference psychrometers / E.M.J. Meijer

230 KNMI contribution to the European project WRINCLE: downscaling relationships for precipitation for several European sites / B.-R. Beckmann and T.A. Buishand

231 The Conveyor Belt in the OCCAM model: tracing water masses by a Lagrangian methodology / Trémeur Balbous and Sybren Drijfhout

232 Analysis of the Rijkoort-Weibull model / Ilja Smits

233 Vectorization of the ECBilt model / X. Wang and R.J. Haarsma

234 Evaluation of a plant physiological canopy conductance model in the ECMWF land surface scheme / J. van de Kassteele

235 Uncertainty in pyranometer and pyrheliometer measurements at KNMI in De Bilt / J.S. Henzing a.o.

236 Recalibration of GOME spectra for the purpose of ozone profile retrieval / Ronald van der A

237 Tracing water masses in the Atlantic / Yann Friocourt and Siebren Drijfhout

238 Klimaat voor Amsterdam Airport Schiphol / A. Smits

239 Seismische analyse van de aardbevingen bij Alkmaar op 9 en 10 september en Bergen aan Zee op 10 oktober 2001 / H.W. Haak, B. Dost, F.H. Goutbeek

240 EBEX-2000 : the KNMI/WAU contribution / W. Kohsiek, E.W. Meijer, P.J.B. Versteeg, O.K. Hartogensis, a.o.

241 Ontwikkeling gidsvergelijkingen voor meerdaagse neerslagkansen / D. Vogelezang en K. Kok

242 On photosynthesis parameters for the A-gs surface scheme for high vegetation / G.J. Steeneveld

243 Temperatuurvergelijkingen voor de Middellange Termijn Gids : ontwikkeling en verificatie over 2000 / J.Wijngaard

244 Verification of clear-air turbulence forecasts / A. Overeem

245 A comprehensive description of the KNMI seismological instrumentation / B. Dost and H. Haak

246 Verandering van neerslagarakteristieken in Nederland gedurende de periode 1901-2001 / A.T.H. Bruin

WETENSCHAPPELIJK RAPPORT = SCIENTIFIC REPORT (WR)

01-01 Hail detection using single-polarization radar / Iwan Holleman

01-02 Comparison of modeled ozone distributions with ozonesonde observations in the tropics / Rob Put

01-03 Impact assessment of a doppler wind lidar in space on atmospheric analyses and numerical weather prediction / G.J. Marseille, A. Stoffelen, F. Bouttier, C. Cardinali, S. de Haan and D. Vasiljevic.

02-01 Quality control and wind retrieval for SeaWinds / M. Potabella and A. Stoffelen

02-02 Shortwave radiation and cloud parameterizations for intermediate complexity models / J.J. Beersma, R. van Dorland and J.D. Opsteeg

02-03 Sensitivity study of the residue method for the detection of aerosols from space-borne sensors / M. de Graaf

02-04 Assimilation of satellite derived surface heating rates in a Numerical Weather Prediction model / Bart van den Hurk and Han The.

02-05 On the use of physical and statistical downscaling techniques for NWP model output / Wim de Rooy and Kees Kok

02-06 ENVISAT Land Surface processes Phase 2 : final report / B.J.J.M. van den Hurk a.o.

KNMI Bibliotheek, postbus 201, 3730 AE De Bilt, tel. 030 - 2 206 855, fax 030 - 2 210 407; bibliotheek@knmi.nl